Bioorganic & Medicinal Chemistry 20 (2012) 5901–5914

Contents lists available at SciVerse ScienceDirect

Bioorganic & Medicinal Chemistry

journal homepage: www.elsevier.com/locate/bmc

Design and synthesis of EGFR dimerization inhibitors and evaluation of their potential in the treatment of psoriasis

Donna Petch [a], Rosaleen J. Anderson [a], Anne Cunningham [a], Suja E. George [a], David E. Hibbs [c], Ran Liu [c], Simon P. Mackay [b], Andrew Paul [b], David A. P. Small [a], Paul W. Groundwater [a,*]

[a] Sunderland Pharmacy School, University of Sunderland, Wharncliffe Street, Sunderland, SR1 3SD, UK
[b] Strathclyde Institute of Pharmacy and Biomedical Sciences, University of Strathclyde, 161 Cathedral Street, Glasgow, G4 0RE, UK
[c] Faculty of Pharmacy, Pharmacy and Bank Building A15, University of Sydney, Sydney, NSW 2006, Australia

ARTICLE INFO

Article history:
Received 31 May 2012
Revised 16 July 2012
Accepted 24 July 2012
Available online 7 August 2012

Keywords:
EGFR dimerization
Xanthines
Psoriasis
Anti-proliferative
Apoptosis

ABSTRACT

Hit compounds from in silico screening for inhibitors of the EGFR dimerization process were evaluated for their anti-proliferative (CCD-1106 keratinocytes) and anti-oxidant (TBA assay) activity and their effect on EGFR dimerization (BS^3 chemical crosslinking assay). 7-Benzyl-8-{*N*′-[1-(3-ethoxy-4-hydroxyphenyl)meth-(*Z*)-ylidene]hydrazino}-1,3-dimethylxanthine **2a** (127 μM) leads to 37% inhibition of p-EGFR dimerization in the CCD-1106 cell line and also inhibits phosphorylation of proteins in the MAPK/ERK pathway, ERK 1/2 and p-38. Based on this initial data, **2a** was selected for further study and was evaluated for its anti-proliferative activity in a range of keratinocyte (CCD-1106, HaCaT and NHEK) and monocyte (ThP1 and U937) cell lines. Xanthine **2a** is pro-apoptotic in HaCaT keratinocytes, as shown by electron microscopy, caspase 3/7, and annexin V-FITC/PI flow cytometric assays. It is significantly less cytotoxic than the established antipsoriatic agent dithranol **14**, as determined by MTT and LDH release assays, and thus has potential as a lead compound for the treatment of psoriasis.

1. Introduction

Psoriasis is a chronic inflammatory disease, which is characterized by the loss of normal cellular homeostasis, resulting in epidermal hyperproliferation, altered differentiation with parakeratosis, and inflammation.[1] It appears in the form of well-demarcated erythematous plaques with a characteristic silvery scaling.[2] Although the pathogenesis of psoriasis is incompletely understood, it has been acknowledged that it originates from T-cell activation and is an autoimmune disease; however the identity of the antigen remains unknown.[3,4] The increased proliferation and abnormal differentiation of keratinocytes is a consequence of the overexpression of growth factors (and their receptors), cytokines, and angiogenic peptides.[4] The treatment of psoriasis relies on well established agents, such as dithranol, acitretin (both of which induce apoptosis but their mechanisms of action are still incompletely understood), cyclosporine (an immunosuppressant which inhibits calcineurin though complexation with cyclophilin) and corticosteroids (which inhibit cytokine, e.g. interleukin-1, production), which have a number of drawbacks in terms of efficacy, toxicity and side-effects, all of which contribute to poor patient compliance. The treatment of moderate to severe psoriasis with traditional systemic agents or phototherapy is associated with a high likelihood of treatment failure—in any year 20% of patients will experience treatment failure/inadequate response to treatment, with the mean time to treatment failure following a change of therapy being 3-6 months.[5] A series of newly developed biologics, for example Ustekinumab (Stelara®), are now used for the treatment of moderate-to-severe plaque psoriasis but the long term effects of these agents has not been established.[6] For example, Efalizumab (Raptiva®), a once-weekly injection for the treatment of severe to moderate plaque psoriasis, was withdrawn due to cases of progressive multifocal leukoencephalopathy (PML) which led to patient deaths.[7]

In comparison with normal skin, increased numbers of epidermal growth factor (EGF) receptors are found in the uppermost layers of skin in active psoriatic lesions,[8] with the EGFR levels (and distribution) returning to normal in regressing lesions. In addition, when skin from non-psoriatic individuals was exposed to EGF in organ culture, histological features which mimic those of psoriatic lesions developed,[9] while inhibition of the EGFR tyrosine kinase ameliorated the psoriatic phenotype in organ-cultured skin, but had no significant effect on the histological features of non-psoriatic skin.[10]

High epidermal levels of EGFR activation are associated with enhanced expression of the pro-inflammatory cytokine, granulocyte/macrophage-colony stimulating factor (GM-CSF), in lesional skin of psoriatic patients.[11] Inhibition of EGFR activity reduced

* Corresponding author. Present address: Faculty of Pharmacy, Pharmacy and Bank Building A15, University of Sydney, Sydney, NSW 2006, Australia.
E-mail address: paul.groundwater@sydney.edu.au (P.W. Groundwater).

0968-0896/$ - see front matter © 2012 Elsevier Ltd. All rights reserved.
http://dx.doi.org/10.1016/j.bmc.2012.07.048

keratinocyte-derived GM-CSF expression both in vitro and in vivo. GM-CSF is key activator of innate immunity and, as such, is involved in chronic stages of inflammatory and autoimmune diseases, such as psoriasis, where macrophages, granulocytes, neutrophils, eosinophils and dendritic cells can contribute to tissue damage and disease.

A number of agents which target the EGFR are currently in clinical use in cancer chemotherapy and these include the small molecule tyrosine kinase inhibitors (gefitinib, erlotinib, and lapatinib) and monoclonal antibodies (e.g. cetuximab and pertuzumab) which target the extracellular domain. The clinical benefits of these agents has been found to be highly variable, as a result of tumor resistance due to variations in the levels of EGFR homo- and hetero-dimerization[12] and mutations in the ATP-binding site of the intracellular tyrosine kinase.[13] However, a number of these EGFR kinase-blocking drugs have been shown to exhibit anti-proliferative and pro-apoptotic activity in keratinocyte lesions[14,15] and improvements in chronic psoriasis for cancer patients receiving EGFR inhibitors have been reported, for example erlotinib,[16] lapatinib,[17] and the anti-EGFR monoclonal antibody cetuximab.[18]

2. Results

2.1. In silico screening and evaluation of EGFR dimerization inhibition

The first step in EGF-stimulated cell proliferation is the binding of EGF to the extracellular portion of its receptor (EGFR), resulting in dimerization, to give an EGF(2):EGFR(2) complex, and the activation of the intracellular protein tyrosine kinase, ultimately leading to signal transduction, DNA synthesis, and cell proliferation.[19]

Our modeling of EGFR dimerization concentrated on key amino acid residues in the dimerization arm (purple) of one monomeric EGFR unit and its binding site (white) for the other EGFR unit, Figure 1, from the crystal structure of the complex of human epidermal growth factor and receptor extracellular domains.[20] Using in silico screening, we have identified potential inhibitors of this interaction, which were then synthesized and tested as potential anti-proliferative agents.

The screening area was refined to the ten main interaction residues of the cleft to which the tip of the 'dimerization arm' binds, Figure 1a. This screen had six queries each made up of six features and, in order for a compound to satisfy a query, it must contain the features stated for that query. This approach was successful, producing 4900 hit compounds with positive LUDI scores from a screen of the Aldrich Rare Chemicals Database (more than 102,000 commercially available drug-like molecules, 75% of which obey all of Lipinski's rules). A number of filters were applied to reduce the number of leads to a more manageable size. Compounds with no chiral centres were initially chosen for ease of synthesis and only compounds with LUDI scores $\geqslant$400 were selected, as these were expected to have greater activity, giving 181 compounds with $M_r \leqslant 500$ and belonging to twenty-one generic structure classes. The data for representatives of the top 5 scoring structure classes **1**–**5** is given in Table 1, Figure 2.

The LUDI scores for each compound are given in Table 1, along with the Ligand Scoring energy when the best conformer of each compound was docked into the EGFR cleft. Each compound was evaluated as an inhibitor of proliferation of the CCD-1106 rapidly proliferating, immortalized keratinocyte cell line (which mimics the hyper-proliferation of the epidermis) using the MTT assay and as an inhibitor of EGFR dimerization (also in this cell line) using an assay involving the chemical crosslinking of the EGFR with BS^3, Figure 3.[21] In this assay, the cells are treated for only 30 min with the test compounds so, in order to observe their effect on dimerization after such a short treatment time, concentrations in the range (118–155 μM) were used, in line with those from a previous study.[21] The effects of these compounds on the phosphorylation levels of some of the proteins (p-ERK1, p-ERK2 and p-p38) involved in the EGFR downstream signaling cascade were also investigated.

All compounds were also evaluated as inhibitors of iron/ascorbate dependent bovine brain lipid peroxidation using the thiobarbituric acid (TBA) test. This assay has also been used in a separate study to test anti-psoriatic compounds for their anti-oxidant activity.[22] The assay was standardized using propyl gallate **6** Figure 4, a commercially available anti-oxidant which gives 70% inhibition at a concentration of 100 μM, as a positive control.

On the basis of its favorable activity profile, Table 1, xanthine **2a** was selected as a lead for the synthesis of further analogues. When CCD-1106 cells were treated with this xanthine **2a** (126 μM for 30 min), levels of the phospho-EGFR dimer decreased by 37%, Figure 3. This xanthine was also a potent anti-oxidant (IC_{50} 8 μM) and significantly reduced the levels of phospho-ERK 1 and 2. Figure 1b shows the best conformer of xanthine **2a** bound to the cleft of the EGFR into which the dimerization arm binds.

2.2. Synthesis and anti-proliferative activity of xanthine analogues 2a–m

In the three step synthesis of the xanthine analogues **2**, substituted benzyl bromides **8** were initially reacted with 8-chlorotheophylline **7** using a literature method[23] to form the 7-benzyl-8-chloroxanthines **9a**–**g** (Scheme 1), which were then reacted with hydrazine hydrate to afford the 7-benzyl-8-hydrazinylxanthines **10a**–**g** in good yield (Scheme 2). In the final step, the

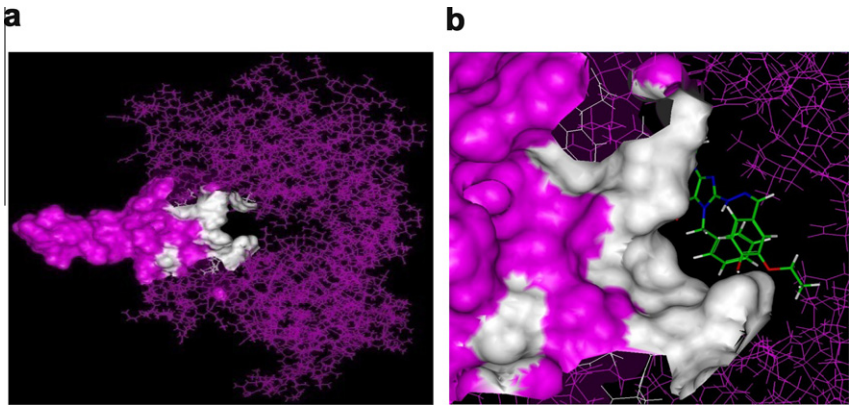

Figure 1. (a) Monomeric EGFR unit, showing dimerization arm (solid purple) and the binding site for the dimerization arm of another EGFR monomer (solid white); (b) A docked stick conformer of **2a** in the cleft of the EGFR dimerization arm binding site.

Table 1
LUDI scores, Ligand scoring docking energies and initial biological testing data of hits **1–5**

Compound	LUDI score	Ligand Scoring docking energy (kcal mol^{-1})	CCD-1106 Anti-prolif. GI_{50} (μM)	Anti-oxid. IC_{50} (mM)	% Inhibition of p-EGFR dimer formation (concn./μM)	% Inhibition of EGFR downstream signaling in CCD-1106 cells (concn./μM)			
						Concn. (μM)	p-ERK 1	p-ERK 2	p-p38
1	536	−37.59	123.35	46.74	52 (155.4)	153.0	28	20	-
2a	478	−54.45	2.69	0.008	37 (126.7)	116.8	39	33	11
3	477	−46.97	4.09	0.40	47 (134.5)	161.1	12	—	-
4	449	−46.58	14.87	3.41	16 (123.6)	120.7	42	33	-
5	426	−66.87	9.33	1.25	42 (118.1)	111.8	26	19	12

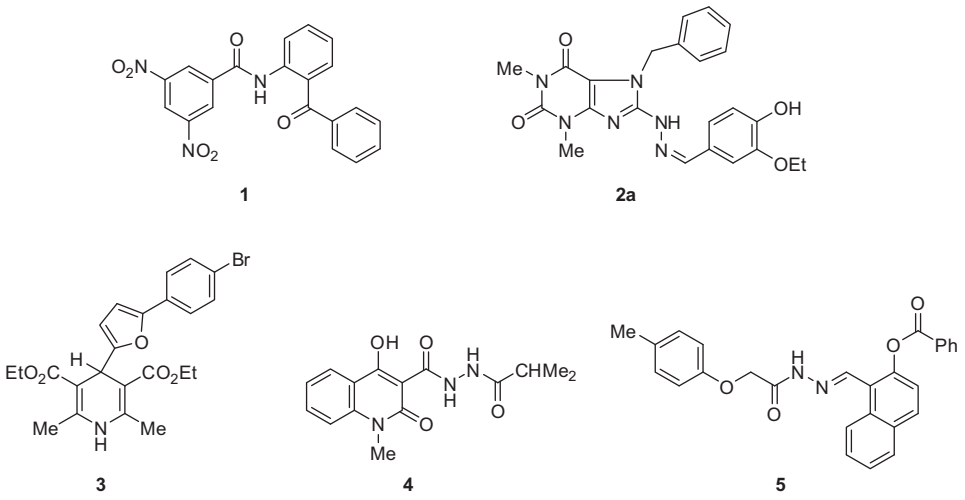

Figure 2. Chemical structures of representatives of the top 5 generic classes of EGFR dimerization hit compounds.

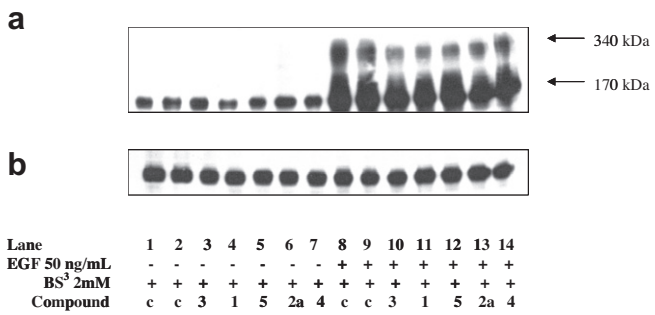

Figure 3. Immunoblots showing; (a) phospho-EGFR levels in CCD-1106 cells, (b) total EGFR. Cells were exposed to compounds for 30 min, then EGF 50 ng/mL for 10 min and BS[3] (extracellular crosslinking agent) 2 mM for 30 min (**c** = control [no added inhibitor]). Immunoblots were quantified by densitometry.

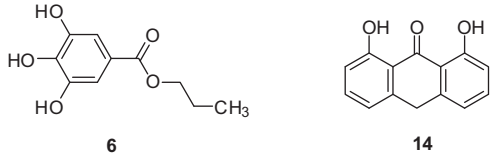

Figure 4. Standards for the anti-proliferative and anti-oxidant assays.

hydrazines **10a–g** were condensed with either 3,4,5-triethoxybenzaldehyde **11a** or 3-ethoxy-4-hydroxybenzaldehyde **11b** to form the 7-benzyl-8-arylidenehydrazinylxanthines **2a–m** in variable yields (Scheme 2). These hydrazinylxanthines **2a–m** were characterized by spectroscopic analysis–the proton of the N=CH group giving a singlet in the ^{1}H NMR spectrum between δ 7.74 and 7.92, and the CH giving a peak in the ^{13}C NMR spectrum between δ 143.4 and 144.6–as well as by elemental analysis.

3,4,5-Triethoxybenzaldehyde **11a** was prepared from the corresponding benzoic acid **12** in a two-step, reduction then oxidation, process via the alcohol **13**, Scheme 2, in 59% overall yield.

The xanthine analogues **2a–m** were initially evaluated for their in vitro anti-proliferative activity in the keratinocyte HPV-16 transformed cell line, CCD-1106, Table 2, using the MTT viability assay. We have previously shown that there were no significant differences between the MTT, NRU (neutral red uptake), SRB (sulforhodamine B), CVS (crystal violet staining), and radioactive [^{3}H]-thymidine incorporation assays for the determination of the dithranol GI_{50} in keratinocytes.[24] The established anti-psoriatic agent dithranol **14**, which had no effect on EGFR dimerization in the crosslinking assay even at a concentration of 348.8 μM, has a GI_{50} of 0.51 ± 0.03 μM in this assay. Dithranol has previously been shown to inhibit keratinocyte proliferation by acting on the EGFR pathway and reducing the binding of EGF to EGFR.[25]

Derivative **2a**, with a GI_{50} of 2.69 μM, was the most active in the assay, but the majority of the other derivatives also showed moderate to high anti-proliferative activity, Table 3. Irrespective of the R^3 and R^4 substituents, a carboethoxy or carboxyl group at R^1 (**2f**,**g**,**l**,**m**) leads to a significant decrease in activity, while both electron-donating and withdrawing R^1 and R^2 substituents can give potent inhibitors.

2.3. Evaluation of the anti-proliferative activity and cytotoxicity of xanthine 2a

On the basis of its activity in the initial screens, derivative **2a** was selected for further biological evaluation and we next investigated its anti-proliferative effect on three different keratinocyte

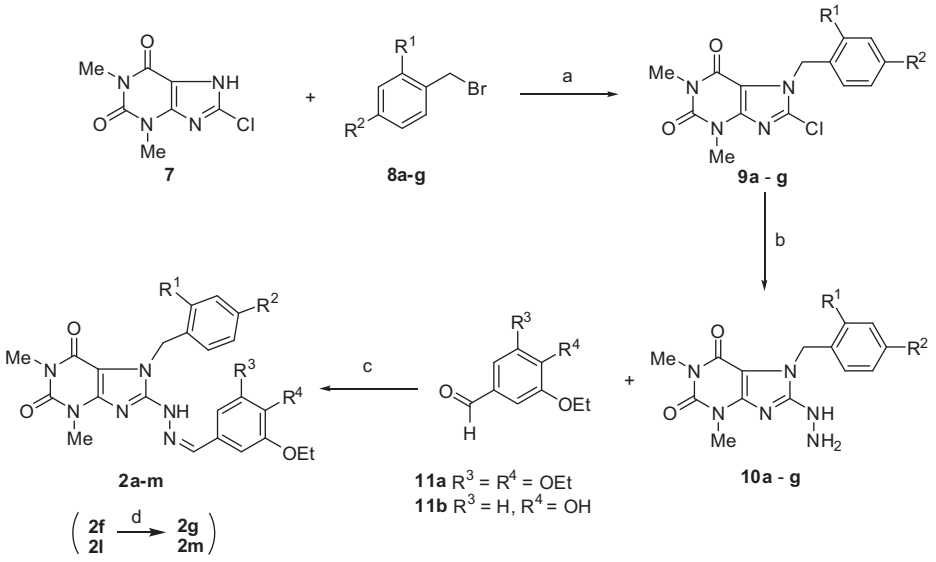

Scheme 1. Reagents and conditions: (a) DMF, K_2CO_3, rt, overnight; (b) EtOH, hydrazine hydrate, reflux, overnight; (c) DCM, DMF, $MgSO_4$, rt, overnight; (d) MeOH, LiOH, reflux, 3 h.

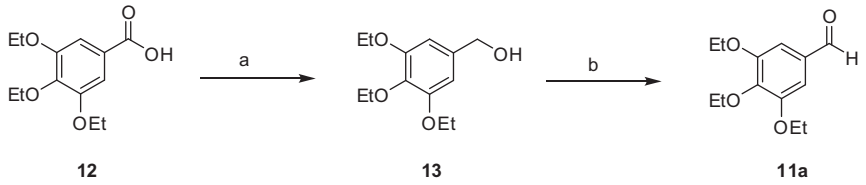

Scheme 2. Reagents and conditions: (a) $LiAlH_4$, Et_2O, reflux, 4.5 h, 88%; (b) PCC, DCM, rt, 4 h, 67%.

Table 2
GI_{50} values in the HPV-16 (E6/E7) transformed cell line, CCD-1106, using the MTT assay for xanthine derivatives **2a–m**

Compound	R^1	R^2	R^3	R^4	Mean GI_{50} (μM) ± S.E.M.[a]
2a	H	H	H	OH	2.69 ± 0.79
2b	H	NO_2	H	OH	5.47 ± 1.53
2c	H	Me	H	OH	9.75 ± 0.12
2d	H	Cl	H	OH	5.21 ± 0.14
2e	NO_2	H	H	OH	8.50 ± 3.06
2f	COOEt	H	H	OH	105.94 ± 2.43
2g	COOH	H	H	OH	178.28 ± 6.48
2h	H	H	OEt	OEt	4.65 ± 1.60
2i	H	NO_2	OEt	OEt	18.91 ± 1.63
2j	H	Me	OEt	OEt	9.83 ± 0.55
2k	OMe	H	OEt	OEt	5.16 ± 0.27
2l	COOEt	H	OEt	OEt	48.26 ± 1.38
2m	COOH	H	OEt	OEt	117.01 ± 2.44

[a] Standard error of the mean (six replicates were performed of each of 8 drug concentrations)

Table 3
Mean GI_{50} values of xanthine **2a** and dithranol **14** in different keratinocyte cell lines using the NRU assay[a]

Cell line/compound	**2a** GI_{50} (μM)	**14** GI_{50} (μM)
CCD-1106	9 ± 0.70	0.40 ± 0.01
HaCaT	22 ± 1.10	0.70 ± 0.02
NHEK	54 ± 0.19	0.50 ± 0.27

[a] Data given as means ± S.E.M., $n = 6$. Incubation period was 72 h.

cell lines; CCD-1106, HaCaT (a rapidly growing, spontaneously transformed human epithelial cell line from adult skin), and normal human epidermal keratinocytes (NHEK; available from pooled donors and representative of 90% of the cells in the epidermis).

Table 4
Mean GI_{50} (μM) values of **2a** compared to dithranol **14** in monocyte cell lines, ThP1 and U937 determined by the Cell Titer 96 AQ_{ueous} one assay[a]

Cell line/compound	Mean GI_{50} (μM) ± S.E.M., $n = 6$	
	2a	**14**
ThP1	36 ± 2.04	54 ± 2.04
U937	46 ± 2.21	5 ± 0.29

[a] Data given as means ± S.E.M., $n = 6$. Incubation period was 72 h.

As can be seen from the data presented in Table 3, xanthine **2a** was less active in all 3 cell lines than the established anti-psoriatic agent dithranol **14**. In the HaCaT cell line, the effects of xanthine **2a** were found to be reversible at the lower concentrations tested.

Xanthine **2a** was also found to inhibit the growth of ThP1 and U937 monocytes in a dose dependent manner, with GI_{50} values of 36 and 46 μM, respectively, Table 4, and had a higher activity than that of dithranol in the ThP1 cell line.

Having thus established the promise of derivative **2a** as an anti-proliferative agent, we next evaluated its cytotoxicity, in the CCD-1106 and HaCaT cell lines, Table 5. The use of the CCD-1106 and HaCaT cell lines as in vitro model systems has the advantages of having no donor specific variations, as found in primary human keratinocytes, as well as providing an almost unlimited supply of identical cells, assuring good reproducibility.

Dithranol **14** was found to be significantly more cytotoxic than xanthine **2a**, particularly in the HaCaT cell line, at both the initial (6 h) and midpoint (24 h) cytotoxicity timepoints, as determined

Table 5
Mean LD_{50} values of xanthine **2a** and dithranol **14** in the CCD-1106 and HaCaT keratinocyte cell lines using a range of endpoints[a]

Compound/assay	Viability assay mean LD_{50} (μM) ± S.E.M., $n = 6$	LDH release assay mean LD_{50} (μM) ± S.E.M., $n = 3$
	MTT	CYTOX-96
CCD-1106		
2a (6 h)	234 ± 4.01	>446
2a (24 h)	112 ± 3.94	>446
14 (6 h)	53 ± 1.17	310 ± 4.81
14 (24 h)	2 ± 0.15	442 ± 10.42
HaCaT		
2a (6 h)	440 ± 6.27	446 ± 5.99
2a (24 h)	446 ± 14.09	446 ± 9.92
14 (6 h)	3 ± 4.78	10 ± 0.34
14 (24 h)	3 ± 0.07	3 ± 0.03

[a] Data given as means ± S.E.M., $n = 6$.

by the viability (MTT) and lactate dehydrogenase (LDH) release assays. These assays have been used extensively to study the toxic effects of agents on a variety of different cell types grown in monolayer cultures.[26,27]

2.4. Evaluation of the pro-apoptotic effects of xanthine 2a in human keratinocytes

Established anti-psoriatic therapies such as dithranol **14**, vitamin-D3 analogues, low-dose methotrexate and PUVA (psoralen plus UVA) induce clinical improvement by the initiation of apoptosis. The pro-apoptotic effects of hydrazinylxanthine **2a** were thus assessed with respect to morphological changes, caspase activation and the binding of annexin V. HaCaT cells exposed to **2a** showed typical apoptotic morphology, with no signs of necrosis by electron microscopy. Xanthine **2a** was found to induce apoptosis in HaCaT keratinocytes after 12 h incubation, through dose-dependent caspase 3/7 activation, Figure 5, resulting in significant caspase 3/7 activation at all the concentrations tested, with remarkably high caspase 3/7 activation even at the lowest concentration tested (25 μg/ml = 55.8 μM). The MTT assay was performed in conjunction with the caspase assay in order to determine if there is any change in the mitochondrial state of the cells during the caspase activation, Figure 5, and the increase in caspase 3/7 activation was always accompanied by a decrease in mitochondrial activity for the cells exposed to **2a**.

In order to quantify the apoptosis induced by **2a** in keratinocytes, HaCaT cells incubated with different concentrations were

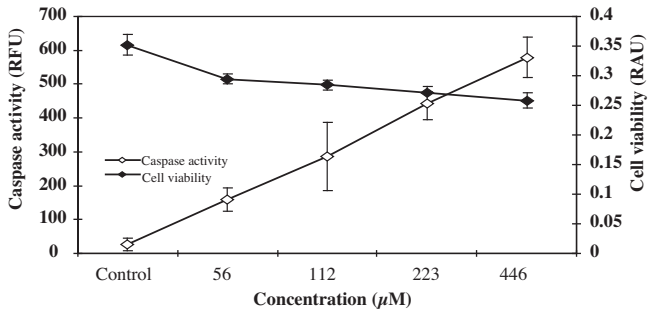

Figure 5. Dose response of caspase 3/7 activity in HaCaT keratinocytes treated with increasing concentrations of **3a** as determined by Apo-ONE homogeneous caspase-3/7 assay. Cell viability was evaluated by the MTT assay in parallel with the caspase 3/7 assays. Keratinocytes were seeded in 96 well microplates at 10,000 cells/0.2 ml/well and allowed to attach overnight. Test compound was added to the cells and incubated for 12 h. MTT and caspase 3/7 assays were performed as described in the experimental section. Data shown represent means ± SEM, $n \geqslant 3$ of two different experiments. Statistical significance between the control and the treated samples was determined by independent *t-test*, $^{*}p < 0.05$.

analysed by flow cytometry, after staining with Annexin V-FITC and PI to measure PS exposure. Figure 6 is representative of the flow cytometry plots obtained from control keratinocytes and drug treated cells after only 9 h exposure, when PS exposure became evident.

3. Discussion

Agents which interfere with the EGFR signaling pathway have potential in the treatment of psoriasis and a number of these EGFR kinase-blocking agents have been shown to exhibit anti-proliferative and pro-apoptotic activity in keratinocyte lesions.[14–16] Half of the amended crystal structure of the EGFR:EGF dimer, 1IVO, was removed to leave just EGFR and its bound EGF ligand. In order to perform an in silico screen for novel inhibitors of the EGFR, the key dimerization interaction residues needed to be highlighted in order to construct a target site for the screen. The eight key residues (Tyr246 to Met253) in the tip of the 'dimerization arm' involved in binding to the cleft of another EGFR during dimerization have previously been identified. The ten key residues in the cleft of the EGFR which bind the tip of the 'dimerization arm' have also been identified.[20,27] These ten residues are Asn86, Phe230, Phe263, Gly264, Ala265, Tyr275, Thr278, Cys283, Arg285 and Ala286. Details of the type of interactions between residues in the tip of the dimerization arm and the cleft of the EGFR have previously been described.[20,28]

LUDI was used to generate an interaction map for the active site, showing three types of interaction sites; hydrogen bond acceptors, donors and hydrophobic (lipophilic) sites. Each of these interaction features were then clustered into groups of hydrogen bond donors (HBD), acceptors (HBA) and hydrophobic (lipophilic) groups and edited to give a manageable number of features. Next, the number of queries and the number of features included in each query were chosen and excluded volumes were added. Excluded volumes are regions into which the screened compounds cannot enter; they include heavy atoms in the protein structure, for example C, N, O, S, but not hydrogen. The chosen queries were then generated and used to screen the *Catalyst* 3D database of compounds. The Aldrich 'Rare Chemical Database' was chosen for the screen, which involved flexible docking of each of the compounds in the database into the defined rigid active site. Only one conformer of each of the compounds was screened to achieve a manageable screening time period. The binding affinity of each of the compounds in the active site was assessed by LUDI, with the greater the LUDI score, the greater the predicted binding affinity of the compound. Each of the ligands was also scored using the Ligand Scoring docking energy for the best conformer (generated by Ligand Fit).

Representatives of the generic structures were then purchased and evaluated for their activity in an EGFR dimerization assay. This assay was recently employed in the discovery of NSC56452 **15**, the first example of a small molecule which targets EGFR dimerization.[21] In common with xanthine **2a**, NSC56452 is a purine derivative and significantly inhibits EGFR dimerization (in this case in CHO cells). NSC56452 inhibits the proliferation of HeLa cells at a concentration of 50 μM but has little effect at lower doses.

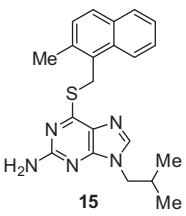

15

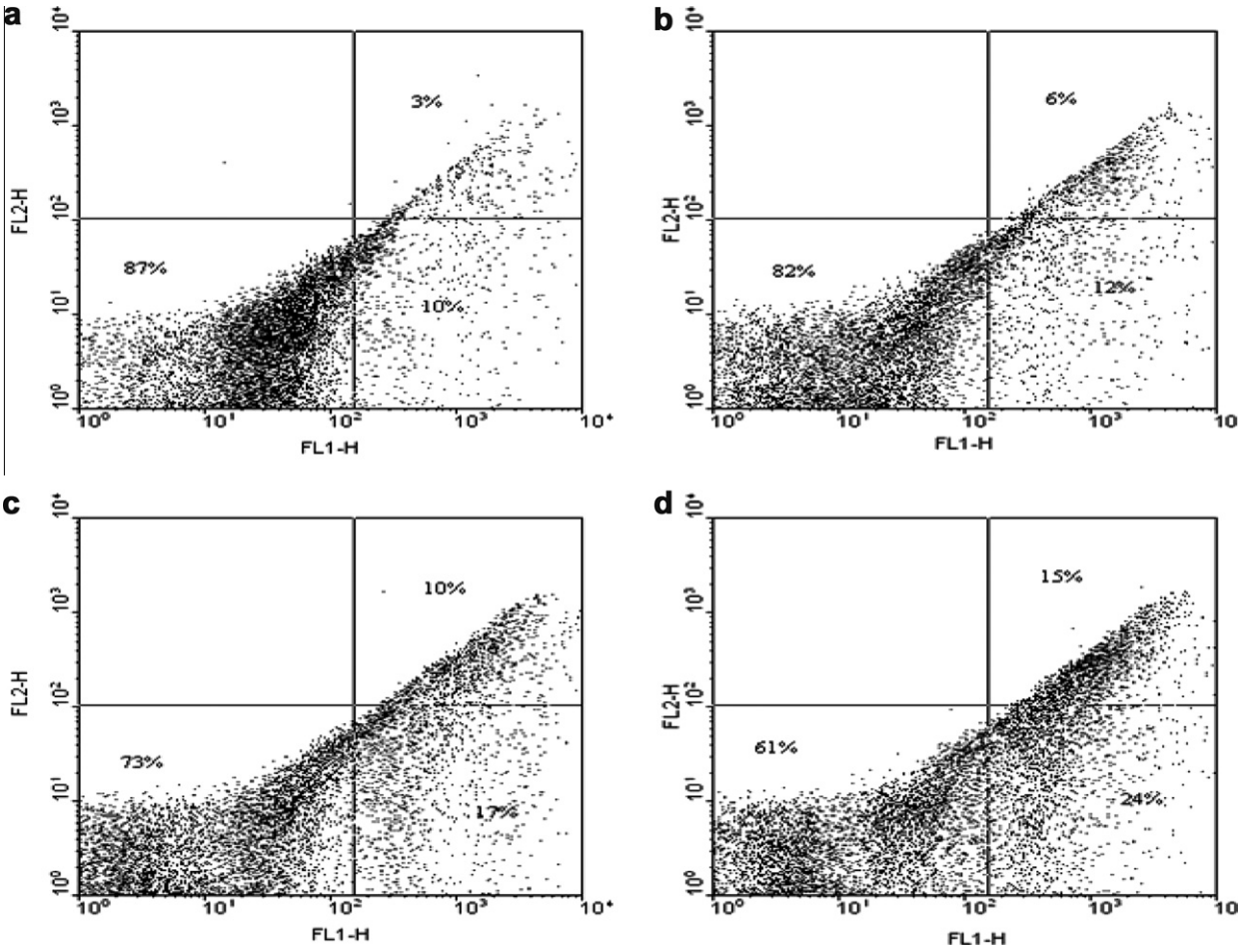

Figure 6. Flow cytometric analysis of apoptosis induced by **2a** in HaCaT keratinocytes. Keratinocytes were seeded at a density of 10^6 cells/ml and allowed to attach overnight. Cells were exposed to different concentrations of the drug; (a) control (vehicle alone), (b) 111.6 μM (c) 223.2 μM and (d) 446 μM. After 9 h incubation, cells were trypsinized, washed and stained with Annexin V-FITC/PI and two-color analysis was performed by flow cytometry. The lower left quadrant ($AnnxV^-/PI^-$) represents viable cells, whereas the lower right quadrant ($AnnxV^+/PI^-$) represents early-phase apoptotic and the upper right quadrant ($AnnxV^+/PI^+$) represents late-phase apoptotic/necrotic cells. The x-axis shows log FL1-fluorescence intensity; the y axis indicates the log FL2-fluorescence intensity. Results are representative of three independent experiments.

Derivative **2a**, with a GI_{50} of 2.69 μM in the anti-proliferative assay, was the most active, but the majority of the other derivatives also showed moderate to high anti-proliferative activity, Table 3. A 3D-QSAR Comparative Molecular Fields Analysis (CoMFA) of the xanthines **2** was performed and the interactions of an active (**2a**) and inactive (**2g**) compound with the CoMFA steric and electrostatic fields are shown in Figures 7a and 7b. As can be clearly seen from Figure 7a, the oxygen of the 3-ethoxy group of the arylhydrazone group of xanthine **2a** lies in a region of negative potential (red) and the interactions of this compound with the steric field are mostly favorable. For the less active xanthine **2g**, Figure 7b, there are no favorable interactions with the electronic field and more unfavorable interactions with the steric field than **2a**. An initial PLS analysis was used to correlate the experimental inhibitory activity of the xanthine growth inhibitors with the CoMFA values containing the magnitude of steric and electrostatic potentials and gave an excellent correlation (R^2 = 0.96).

Chronic inflammation is a pathological feature of psoriasis and reactive oxygen species (ROS) and increased oxidative stress are believed to be linked to inflammation.[29–31] An anti-psoriatic drug with anti-oxidant properties thus has great potential to aid in the treatment of skin inflammation. With this in mind, all of the hit compounds were also tested for their anti-oxidant activity. Xanthine **2a** is a potent anti-oxidant (IC_{50} 8 μM in the TBA assay) and this data, along with that for its activity in the EGFR dimerization, downstream signaling (p-ERK 1, p-ERK2 and p-p38), and CCD-1106 growth inhibition assays (Table 1), was used to select xanthine **2a** for further biological evaluation.

Monocyte cell lines are commonly used as in vitro models for inflammatory disorders in the study of the effects of pro-inflammatory cytokines. Although monocytes or macrophages can be obtained from humans, they present many difficulties, such as sample acquisition, donor variability and the difficulty associated with obtaining a homogeneous population of human monocytes in the amounts required for pre-clinical studies. In order to overcome the problems associated with sample acquisition and donor variability, monocyte cell lines such as ThP1 and U937 have been used extensively as models for primary monocytes[32] and the appropriateness of using ThP1 and U937 cell lines as models for primary peripheral blood monocytes (PBMs) for studying inflammatory disorders has previously been demonstrated.[33,34] Several studies have shown that monocyte cell lines are a sensitive target for successful anti-psoriatic agents, such as dithranol,[35,36] methotrexate,[37,38] cyclosporin A,[39] and corticosteroids.[40] The novel xanthine **2a** was found to be effective in inhibiting the growth of both the monocyte cell lines, with a higher activity than that of dithranol **14** in the ThP1 cell line.

Analysis of the cytotoxicity of xanthine **2a** was performed at 6 h and 24 h in order to determine the concentrations of test agents causing initial cytotoxicity (6 h) and those causing midpoint

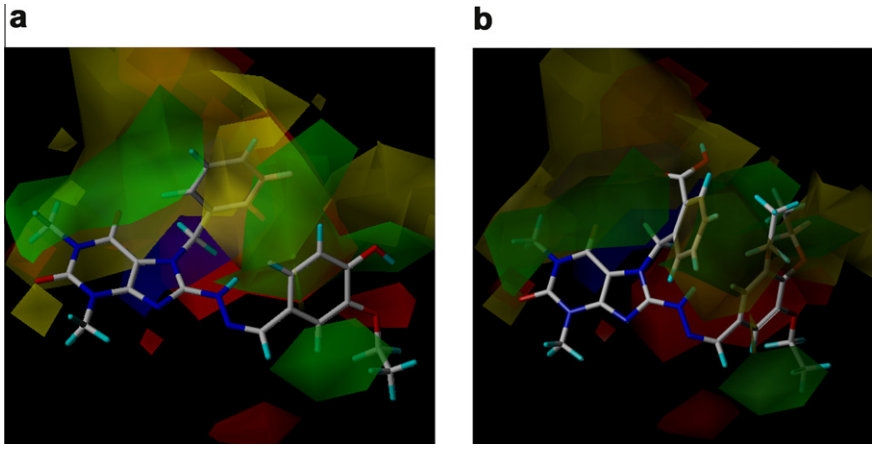

Figure 7. (a) Interaction of the CoMFA steric and electrostatic fields SD × coeff contour maps with 'active' xanthine **2a**; (b) Interaction of the CoMFA steric and electrostatic fields SD × coeff contour maps with 'inactive' xanthine **2g**. Bulky groups in the green region favor the inhibitory activity, but bulky groups in the yellow region are not favorable. Negative potentials in the red region favor the inhibitory activity, but negative potentials in the blue region are not desirable.

cytotoxicity (24 h). Such comparative data is very informative of the kinetics of the cytotoxicity curves. The MTT assay is a measure of mitochondrial reductase activity, and the CYTOX-96 assay determines lactate dehydrogenase (LDH) release and so can be used to determine cell membrane damage (one of the final stages of cell death). Korting et al. have confirmed that there is a close correlation between the in vitro cytotoxicity values predicted by viability assays in cultured human foreskin keratinocytes and the in vivo irritancy data.[41]

A severe disadvantage of permeability assays is that the initial damage sites of many cytotoxic agents are intracellular.[42] Cells may, therefore, be irreversibly damaged and committed to die but the plasma membrane may still be intact. These assays are thus likely to underestimate cellular damage caused by the cytotoxic agents in comparison to other methods. The LDH release assay, which is based on the measurement of cytoplasmic enzymes released by injured cells, is very informative, not only of cell growth inhibition, but also of the extent of cell lysis caused by test agents.[43] It was observed that the cytotoxicity of **2a** was detected earliest by measuring the metabolic activities of the cells, whereas the LDH leakage assay seems to be the most definitive marker of cell death by membrane rupture. Dithranol **14** has greater growth inhibitory activity in all 3 of the keratinocyte cell lines tested but compound **2a** proved to be much less cytotoxic than dithranol **14** in all cases, while there was no difference between the initial and midpoint toxicities for **2a** in the MTT viability assay in the HaCaT cell line, or the LDH release assay in either cell line.

Several studies have been carried out which have investigated the role played by defective apoptosis in the pathogenesis of psoriasis. Experimental studies have revealed that keratinocytes derived from psoriatic epidermis display resistance to apoptotic stimuli, unlike the healthy keratinocytes of normal skin.[44] Cathepsin D and zinc-α_2-glycoprotein, catalytic enzymes linked with apoptosis and flaking of the skin, are present within the stratum corneum of normal skin, but are missing in psoriatic plaques.[45] An inverse reaction of psoriatic keratinocytes in response to IFN-γ has also been reported. In normal keratinocytes, IFN-γ upregulates the expression of Cathepsin D and zinc-α_2-glycoprotein, while they are down regulated in keratinocytes from psoriatic epidermis.[45] Furthermore, expression of Bcl-2 is found to be increased in psoriatic epidermis.[46] Other studies have revealed an apoptotic index of 0.12% in healthy skin, of 0.035% in psoriatic epidermis and of 0.31% in regressing psoriasis after PUVA treatment and this underlines the fact that loss of apoptosis within the epidermis could be of some pathologic relevance for the development of psoriatic hyperplasia.[47] Apoptosis in psoriatic keratinocytes has, in addition, been shown to be dysregulated at the cytokine level; it has recently been shown that IL-15 does not display any relevant effects in cell proliferation, but inhibits both the anti-Fas and the methylcellulose-induced apoptosis of keratinocytes in vitro.[48] Interestingly, increased expression of IL-15 was observed in the epidermis of lesional psoriatic skin.[48] It has been shown that several genes which were reported to be related to apoptosis or anti-proliferation show high expression levels only in uninvolved psoriatic lesions.[49] All psoriatic biopsies revealed absent apoptotic keratinocytes and lymphocytes and these results are in agreement with previous studies, where no apoptotic cells were detected in any of the psoriatic lesions.[47,49]

In order to identify the cellular changes, the morphological differences between the normal control and the treated cells were compared by electron microscopy. Compared to the untreated control, cells treated with **2a** exhibited typical morphological characteristics of early phase apoptosis and late phase apoptosis/necrosis, including; chromatin rearrangements and condensation, nuclear fragmentation, an intact membrane and cytoplasm, the formation of apoptotic bodies and cytoplasmic vacuolization, surface blebbing and formation of apoptotic bodies. Cells undergoing necrosis displayed nuclei with a nuclear pattern resembling that of a normal cell but a degenerated cytoplasm and membranes as well as clumped chromatin, swelling and the appearance of lesions on the cell surface.

Apoptotic cell death is characterized by numerous morphological and biological changes. One of the features of apoptotic cells is the loss of cell membrane asymmetry during the early phases of programed cell death. Phosphatidylserine (PS), a phospholipid that can only be found in the inner layer of the intact cell membrane, becomes exposed to the outer leaflet, where it can be detected by the selective binding of Annexin V to PS under defined salt and calcium concentrations and it is, therefore, considered to be an early marker of apoptosis. Cells in the early phase of apoptosis bind Annexin V (AnnxV) but exclude propidium iodide (PI). On the other hand, double positive cells (stained by both Annexin V-FITC and PI) may represent a late apoptotic/necrotic population, since necrotic cells lose membrane integrity and cannot exclude PI. Flow cytometric analysis of cells stained with Annexin V-FITC and PI allows the identification of intact (unstained), apoptotic ($AnnxV^+/PI^-$) and necrotic ($AnnxV^+/PI^+$) populations.

Treatment with **2a** resulted in a slow but steady increase in the number of both early apoptotic and late apoptotic/necrotic cells, accompanied by a decrease in the number of viable cells, Figures 6 and 8. A significant increase in the number of early apoptotic and late apoptotic/necrotic cells was observed for the

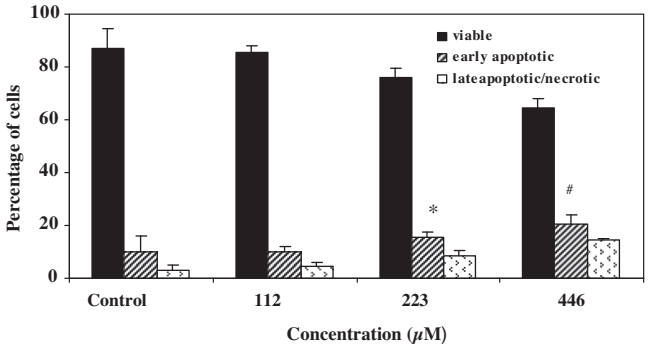

Figure 8. Effect of xanthine **2a** on the induction of apoptosis and necrosis in human keratinocytes. Cells were seeded at a density of 10^6 cells/ml and allowed to attach overnight. Cells were exposed to different concentrations of the drug for 9 h. after the incubation period, cells were then trypsinized, washed and stained with Annexin V-FITC/PI and two-color analysis was performed by flow cytometry. Data shown represent means ± SEM, $n \geqslant 3$ of two different experiments. Statistical significance between the control and the treated samples were determined by independent *t*-test, $^{*}p < 0.05$ and $^{\#}p < 0.01$.

concentration range tested, with the increase being more pronounced at the highest concentration, Figure 8. As the incubation period for these studies was only 12 h (compared to the 72 h incubation times for the growth inhibition assays), the concentrations chosen for these apoptosis studies were greater than the GI_{50}, but well below the LD_{50}, as it would be difficult to detect any effects with lower concentrations after such a short incubation time.

The Annexin V-FITC/PI flow cytometric assays provided quantitative information about the apoptotic process and, in agreement with the electron microscopy observations, **2a** was found to induce apoptosis in keratinocytes. The percentage of cells in the late apoptotic/necrotic phase was observed to be low (15%), even at the highest concentration (446 μM) tested, indicating that the compound has very low cytotoxicity. This was also supported by the viability assay (MTT), Figure 5, which showed 62% viability after 12 h incubation with a high concentration (446 μM) of **2a**.

4. Conclusion

In conclusion, based on the results from growth inhibition assays in human keratinocytes and monocytes and an anti-oxidant assay, xanthine **2a** was identified as a potential agent for the treatment of psoriasis. This xanthine inhibits the growth of keratinocytes and monocytes and is significantly less cytotoxic than the established antipsoriatic agent dithranol **14**. These findings were further confirmed by electron microscopy, caspase 3/7 assays, and flow cytometric analysis which showed that this novel compound induces apoptosis in highly proliferating human keratinocytes and is, therefore, therapeutically relevant for the treatment of psoriasis.

5. Experimental

5.1. General

Melting points were determined on a Stuart Scientific SMP10 apparatus and are uncorrected. IR spectra were recorded on an ATl Mattson Generis series FTIR or Unicam Research series 1 FTIR using KBr disks or on a Perkin Elmer Inc Spectrum BX FT-IR system. ^{1}H NMR spectra were recorded in DMSO or $CDCl_3$ on a Bruker AVANCE 300 or 500, at 300 MHz or 500 MHz. Coupling constants are given in Hz and all chemical shifts, which are relative to the peaks for residual protonated solvent, are given in ppm. ^{13}C NMR spectra were obtained on the AVANCE 300 or 500 at 75 or 125 MHz, respectively. Column chromatography was performed using Fluka silica gel 60. Thin layer chromatography was performed using Merck aluminum sheets, silica gel 60 F_{264}. Mass spectrometry was performed on an Esquire 3000plus or Bruker ApexII, for low and high resolution spectra, respectively. Elemental analyses were performed by Medac Ltd, Brunel Science Centre, Surrey, United Kingdom or on an Exeter Analytical CE-440 elemental analyser at Chemispec, University of Sunderland, United Kingdom.

Dimethylsulfoxide (DMSO), trypan blue, and MTT were purchased from Sigma–Aldrich, Dorset, UK. Alamar blue was obtained from Serotec (Oxford, UK). Phosphate buffered saline (PBS) was purchased from Gibco, Renfrewshire, UK. An HPV-16 immortalised human keratinocyte cell line obtained from the American Tissue Culture Collection (ATCC), CRL-2309 and reference CCD-1106 KERTr was used. Keratinocyte serum free medium (SFM) purchased from Gibco, was used successfully in previous studies to cultivate a HPV-16 cell line[50,51] and was used in this study. The keratinocyte growth supplements bovine pituitary extract (BPE) and epidermal growth factor (rEGF) were purchased from Gibco. Cells were grown under conditions of 5% CO_2 at 37 °C. Manipulation of the cells was performed in a Class II Safety Cabinet under aseptic conditions.

Cell Titer 96 Aqueous One solution cell proliferation assay kit, and Cyto Tox 96 assay kits were purchased from Promega (Madison, USA). Annexin V-FITC (K101-100) was obtained from Biovision (Mountain View, CA) and the caspase-3/7 activity assay kit from Promega (Madison, WI). p-EGFR (Tyr1173): sc-12351, p-ERK (E-4): sc-7383 and p-p38 [D-8] antibodies were purchased from Santa Cruz Biotechnology, Santa Cruz, CA, USA.

5.2. In silico screening

The crystal structure of the EGFR:EGF 2:2 dimer, determined by X-ray diffraction, was obtained from the *RCSB protein databank* (1IVO).[20] *Insight II* 2005, *Cerius*^{2} 4.10L, *Catalyst* 4.10 and *DS ViewerPro* 6.0 programs from Accelrys were used with a Silicon or Linux Graphics workstation. The force field used in *Insight II* was CFF91 and for *Cerius*^{2} was CFF. The compound database screened was the Aldrich 'Rare Chemicals Database' (SALOR). All modeling images were taken from screen shots using *Insight II* or *DS ViewerPro* 6.0.

The crystal structure of the EGFR:EGF dimer, 1IVO, was amended for use by adding hydrogens and removing all water molecules and NAG ligands. An assembly was created including three subsets; all atoms (heavy), backbone, and backbone and side chains, then the structure were minimised using *Insight II Discover* module.

Half of the amended crystal structure dimer was removed to leave just EGFR and its bound EGF. The binding site to be screened was defined by entering the coordinates of the centre of the site and radius by highlighting the ten key binding residues of the 'cleft'. Next, *LUDI* was used to generate an interaction map for the active site, showing three types of interaction sites; hydrogen bond acceptors, donors and hydrophobic (lipophilic) sites. Each of these interaction features were then clustered into groups of hydrogen bond donors (HBD), acceptors (HBA) and hydrophobic (lipophilic) groups and edited to give a manageable number of features. The number of queries and the number of features included in each query were chosen and excluded volumes were added. The chosen queries were then generated and used to screen the *Catalyst* 3D database of the Aldrich 'Rare Chemical Database', containing 102,000 compounds. This screen involved flexible docking of each of the compounds in the database into the defined rigid active site. Only one conformer of each of the compounds was screened to achieve a manageable screening time period. The binding affinity of each of the compounds in the active site was assessed by *LUDI*. Each compound was given a LUDI score to represent the predicted

binding affinity and this score was used to prioritise the lead compounds. This LUDI score uses the same algorithms as the LUDI 1 score of the program Ligand Scoring. The greater the LUDI score, the greater the predicted binding affinity of the compound.

5.3. Synthetic chemistry

5.3.1. 3,4,5-Triethoxybenzaldehyde (11a)

5.3.1.1. 3,4,5-Triethoxyphenylmethanol (13). 3,4,5-Triethoxybenzoic acid **12** (5.03 g, 19.77 mmol) was added slowly to an ice-cooled grey suspension of $LiAlH_4$ (1.42 g, 37.41 mmol) in dry diethyl ether (50 mL). The mixture was then refluxed for 4.5 h. The suspension was cooled, quenched with water/ethyl acetate (100 mL 1:1) and filtered through celite. The organic layer was separated, dried over $MgSO_4$, filtered and the solvent evaporated under reduced pressure to give (3,4,5-triethoxyphenyl)methanol, **13** as an off-white solid (4.20 g, 88%); mp 38–39 °C (lit. mp 29–30 °C);[52] R_f = 0.38 (pet.ether/ethyl acetate 1:1); ν_{max} (KBr)/cm^{-1} 3283 (OH), 1585 (Ar C=C), 1436 (Ar C=C); ^{1}H NMR (300 MHz, DMSO): δ 1.13 (3H, t, J = 6.9 Hz, CH_3), 1.23 (6H, t, J = 6.9 Hz, 2 × CH_3), 3.81 (2H, q, J = 6.9 Hz, CH_2), 3.91 (4H, q, J = 6.9 Hz, 2 × CH_2), 4.31 (2H, d, J = 5.7 Hz, CH_2), 4.99 (1H, s, OH), 6.49 (2H, s, H-2,6); ^{13}C NMR (75 MHz, DMSO): δ 15.3 (2 × CH_3), 15.9 (CH_3), 63.5 (CH_2), 64.4 (2 × CH_2), 68.2 (CH_2), 105.2 (2 × CH), 136.2 (quat.), 138.4 (quat.), 152.7 (2 × quat.); Anal. Calcd for $C_{13}H_{20}O_4$: C, 65.0; H, 8.4. Found: C, 64.9; H, 8.4.

5.3.1.2. 3,4,5-Triethoxybenzaldehyde (11a). To a mixture of PCC (2.15 g, 9.9 mmol) and powdered molecular sieves (3 Å, 1.30 g) in dry CH_2Cl_2 (20 mL) was added (3,4,5-triethoxyphenyl)methanol **9** (1.60 g, 6.7 mmol) at 0 °C. The reaction mixture was stirred at room temperature for 4 h. The solvent was evaporated and diethyl ether (10 mL) was added. The slurry was stirred and filtered through celite and the solvent was evaporated under reduced pressure to produce 3,4,5-triethoxybenzaldehyde **10** as pale brown crystals (1.06 g, 67%); mp 67–69 °C (lit. mp 68 °C);[53] R_f = 0.71 (pet.ether/ethyl acetate 1:1); ν_{max} (KBr)/cm^{-1}; 1685 (C=O), 1583 (Ar C=C), 1439 (Ar C=C), 1120 (C–O), 1100 (C–O); ^{1}H NMR (300 MHz, DMSO): δ 1.16 (3H, t, J = 6.9 Hz, CH_3), 1.27 (6H, t, J = 6.9 Hz, 2 × CH_3), 3.62 (2H, q, J = 6.9 Hz, CH_2), 4.02 (4H, q, J = 6.9 Hz, 2 × CH_2), 7.11 (2H, s, H-2,6), 9.76 (1H, s, CHO); ^{13}C NMR (75 MHz, DMSO): δ 15.1 (2 × CH_3), 15.9 (CH_3), 64.7 (2 × CH_2), 68.7 (CH_2), 108.1 (2 × CH), 131.9 (quat.), 142.9 (quat.), 153.3 (2 × quat.), 192.3 (CHO); Anal. Calcd for $C_{13}H_{18}O_4$: C, 65.5; H, 7.6. Found: C, 65.6; H, 7.6.

5.3.2. General procedure for the synthesis of 7-benzyl-8-chloro-1,3-dimethylxanthine (9a) and analogues (9b–g)

7-Benzyl-8-chloroxanthines **9a–g** were prepared by the method of Vollmann and Müller.[23] 8-Chlorotheophylline **7** (10 mmol) was added to dry dimethylformamide (30 mL) then K_2CO_3 (20 mmol) and the appropriate benzyl bromide **8** (20 mmol) were added and the reaction mixture was stirred overnight at room temperature. Water (60 mL) was added and the reaction mixture was cooled in ice for 2 h. The precipitated product was collected by vacuum filtration, washed with water (10 mL) and dried in a vacuum oven to give the 8-chloroxanthine **9a–g**.

5.3.3. General procedure for the synthesis of 7-benzyl-8-hydrazino-1,3-dimethylxanthine (10a) and analogues (10b–g)

To a warm solution of xanthine **10a–g** (1.65 mmol) in ethanol (20 mL), hydrazine hydrate (0.10 mL, 3.30 mmol) was added. The reaction mixture was then refluxed overnight. After cooling, the precipitate formed was filtered under suction, washed with cold ethanol, recrystallized from methanol and acetonitrile and dried in a vacuum oven to give the hydrazine.

5.3.4. General procedure for the synthesis of 7-benzyl-8-{*N*′-[1-(3-ethoxy-4-hydroxyphenyl)meth-(*Z*)-ylidene]hydrazino}-1,3-dimethylxanthine (2a) and analogues (2b–m)

To a stirred suspension of aldehyde **11a** or **11b** (0.50 mmol) in dichloromethane (5 mL) and hydrazine **10a–g** (0.50 mmol), *N,N*-dimethylformamide was added dropwise until a clear solution was formed. Magnesium sulfate (0.1 g) was added and the reaction mixture was stirred overnight at room temperature. The magnesium sulfate was filtered from the reaction solution, the solvents were removed under reduced pressure, and the residue recrystallized from methanol and acetonitrile to afford the product.

5.3.4.1. 7-Benzyl-8-{N′-[1-(3-ethoxy-4-hydroxyphenyl)meth-(*Z*)-ylidene]hydrazino}-1,3-dimethylxanthine (2a). Prepared from 3-ethoxy-4-hydroxybenzaldehyde **11b** (0.61 g, 3.60 mmol) and 7-benzyl-8-hydrazino-1,3-dimethyl-3,7-1*H*-dihydropurine-2,6-dione **10a** (0.99 g, 3.29 mmol), 7-benzyl-8-{*N*′-[1-(3-ethoxy-4-hydroxylphenyl)meth-(*Z*)-ylidene]hydrazine}-1,3-dimethyl-3,7-1*H*-dihydropurine-2,6-dione **2a** was obtained as pale brown crystals (1.04 g, 70%); R_f = 0.50 (ethyl acetate); mp 243–244 °C; ν_{max} (KBr)/cm^{-1} 3512 (NH), 3403 (OH), 1693 (C=O), 1653 (C=O), 1621 (Ar C=C), 1477 (Ar C=C), 1286 (C–O); ^{1}H NMR (300 MHz, DMSO): δ 1.29 (3H, t, J = 6.9 Hz, CH_3), 3.17 (3H, s, N^1-CH_3), 3.40 (3H, s, N^3-CH_3), 3.81 (2H, q, J = 6.9, CH_2), 5.80 (2H, s, CH_2), 6.77 (1H, d, J = 8.2 Hz, H-5), 6.89 (1H, dd, J = 8.2, 1.5 Hz, H-6), 6.99 (1H, d, J = 1.5 Hz, H-2), 7.18–7.41 (5H, m), 7.90 (1H, s, CH), 9.32 (1H, s, NH), 11.49 (1H, s, OH); ^{13}C NMR (75 MHz, DMSO): δ 15.4 (CH_3), 28.2 (CH_3), 30.2 (CH_3), 48.8 (NCH_2), 64.6 (CH_2), 103.4 (quat.), 110.8 (CH), 116.3 (CH), 121.9 (CH), 126.5 (quat.), 127.3 (2 × CH), 128.0 (CH), 129.3 (2 × CH), 138.8 (quat.), 144.5 (CH), 147.9 (quat.), 149.2 (quat.), 149.5 (quat.), 151.1 (quat., C=O), 151.9 (quat.), 153.9 (quat., C=O); Anal. Calcd for $C_{23}H_{24}N_6O_4$: C, 61.6; H, 5.4; N, 18.7. Found: C, 61.4; H, 5.4; N, 18.6.

5.3.4.2. 8-{N′-[1-(3-Ethoxy-4-hydroxyphenyl)meth-(*Z*)-ylidene]hydrazino}-1,3-dimethyl-7-(4-nitrobenzyl)xanthine (2b). Prepared from 3-ethoxy-4-hydroxybenzaldehyde **11b** (0.55 g, 3.25 mmol) and 8-hydrazino-1,3-dimethyl-7-(4-nitrobenzyl)-3,7-1*H*-dihydropurine-2,6-dione **10b** (0.99 g, 2.90 mmol), 8-{*N*′-[1-(3-ethoxy-4-hydroxyphenyl)meth-(*Z*)-ylidene]hydrazino}-1,3-dimethyl-7-(4-nitrobenzyl)-3,7-1*H*-dihydropurine-2,6-dione **2b** was obtained as yellow crystals (0.64 g, 49%); R_f = 0.41 (ethyl acetate); mp 267–268 °C; ν_{max} (KBr)/cm^{-1} 3436 (NH), 3069 (OH), 1685 (C=O), 1619 (C=O), 1596 (Ar C=C), 1525 (NO_2), 1508 (Ar C=C), 1332 (NO_2), 1268 (C–O); ^{1}H NMR (300 MHz, DMSO): δ 1.28 (3H, t, J = 6.9 Hz, CH_3), 3.18 (3H, s, N^1-CH_3), 3.42 (3H, s, N^3-CH_3), 3.74 (2H, q, J = 6.9 Hz, CH_2), 5.90 (2H, s, CH_2), 6.69–6.77 (2H, m), 6.82 (1H, d, J = 1.5 Hz, H-2), 7.45 (2H, d, J = 8.7 Hz, H-2′,6′), 7.86 (1H, s, CH), 8.13 (2H, d, J = 8.7 Hz, H-3′,5′), 8.98 (1H, bs, NH), 11.43 (1H, s, OH); ^{13}C NMR (75 MHz, DMSO): δ 14.9 (CH_3), 27.6 (CH_3), 29.7 (CH_3), 48.4 (NCH_2), 64.2 (CH_2), 103.1 (quat.), 110.2 (CH), 115.7 (CH), 121.6 (CH), 123.8 (2 × CH), 125.9 (quat.,), 127.9 (2 × CH), 144.6 (CH), 146.1 (quat.), 147.1 (quat.), 147.4 (quat.), 148.8 (quat.), 149.1 (quat.), 150.8 (quat., C=O), 151.5 (quat., C-8), 153.5 (quat., C=O, C-6); Anal. Calcd for $C_{23}H_{23}N_7O_6$: C, 55.9; H, 4.7; N, 19.9. Found: C, 55.9; H, 4.7; N, 19.9.

5.3.4.3. 8-{N′-[1-(3-Ethoxy-4-hydroxyphenyl)meth-(*Z*)-ylidene]hydrazino}-1,3-dimethyl-7-(4-methylbenzyl)xanthine (2c). Prepared from 3-ethoxy-4-hydroxybenzaldehyde **11b** (0.59 g, 3.51 mmol) and 8-hydrazino-1,3-dimethyl-7-(4-methylbenzyl)-3,

7-1*H*-dihydropurine-2,6-dione **10c** (0.99 g, 3.17 mmol), 8-{N′-[1-(3-ethoxy-4-hydroxyphenyl)meth-(*Z*)-ylidene]hydrazino}-1,3-dimethyl-7-(4-methylbenzyl)-3,7-1*H*-dihydropurine-2,6-dione **2c** was obtained as pale yellow solid (0.59 g, 40%); R_f = 0.56 (pet. ether/ethyl acetate, 1:9); mp 195–198 °C; ν_{max} (KBr)/cm^{-1} 3654 (NH), 3220 (OH), 1689 (C=O), 1624 (C=O), 1578 (Ar C=C), 1480 (Ar C=C), 1273 (C–O); ^{1}H NMR (300 MHz, DMSO): δ 1.20 (3H, t, J = 7.2 Hz, CH_3), 2.14 (3H, s, CH_3), 3.08 (3H, s, N^1-CH_3), 3.30 (3H, s, N^3-CH_3), 3.71 (2H, q, J = 7.2 Hz, CH_2), 5.65 (2H, s, CH_2), 6.67 (1H, d, J = 8.4 Hz, H-5), 6.81 (1H, dd, J = 8.4, 1.8 Hz, H-6), 6.91 (1H, d, J = 1.8 Hz, H-2), 6.96–7.04 (4H, m), 7.81 (1H, s, CH), 9.20 (1H, s, NH), 11.36 (1H, s, OH); ^{13}C NMR (75 MHz, DMSO): δ 15.1 (CH_3), 21.1 (CH_3), 27.8 (CH_3), 29.8 (CH_3), 48.2 (NCH_2), 64.1 (CH_2), 103.0 (quat.), 110.3 (CH), 116.0 (CH), 121.6 (CH), 126.2 (quat.), 127.0 (2 × CH), 129.4 (2 × CH), 135.4 (quat.), 136.8 (quat.), 144.0 (CH), 147.6 (quat.), 148.8 (quat.), 149.1 (quat.), 150.7 (quat., C=O), 151.5 (quat.), 153.5 (quat., C=O); Anal. Calcd for $C_{24}H_{26}O_4N_6$: C, 62.3; H, 5.7; N, 18.2. Found: C, 62.0; H, 5.7; N, 18.1.

5.3.4.4. 7-(4-Chlorobenzyl)-8-{N′-[1-(3-ethoxy-4-hydroxyphenyl) meth-(*Z*)-ylidene]hydrazino}-1,3-dimethylxanthine (2d).

Prepared from 3-ethoxy-4-hydroxybenzaldehyde **11b** (0.55 g, 3.26 mmol) and 8-hydrazino-1,3-dimethyl-7-(4-chlorobenzyl)-3,7-1*H*-dihydropurine-2,6-dione **10d** (0.66 g, 1.97 mmol), 8-{N′-[1-(3-ethoxy-4-hydroxyphenyl)meth-(*Z*)-ylidene]hydrazino}-1,3-dimethyl-7-(4-chlorobenzyl)-3,7-1*H*-dihydropurine-2,6-dione **2d** was obtained as a fine cream solid (0.90, 95%); R_f = 0.54 (ethyl acetate); mp 266–267 °C; ν_{max} (KBr)/cm^{-1} 3492 (NH), 3231 (OH), 1690 (C=O), 1655 (C=O), 1621 (Ar C=C), 1513 (Ar C=C), 1276 (C–O); ^{1}H NMR (300 MHz, DMSO): δ 1.31 (3H, t, J = 6.9 Hz, CH_3), 3.18 (3H, s, N^1-CH_3), 3.41 (3H, s, N^3-CH_3), 3.77 (2H, q, J = 6.9 Hz, CH_2), 5.77 (2H, s, CH_2), 6.74 (1H, d, J = 8.1 Hz, H-5), 6.84 (1H, dd, J = 8.1, 1.8 Hz, H-6), 6.92 (1H, d, J = 1.8 Hz, H-2), 7.22 (2H, d, J = 8.7 Hz, H-2′,6′), 7.31 (2H, d, J = 8.7 Hz, H-3′,5′), 7.90 (1H, s, CH), 9.17 (1H, bs, NH), 11.43 (1H, s, OH); ^{13}C NMR (75 MHz, DMSO): δ 15.0 (CH_3), 27.7 (CH_3), 29.7 (CH_3), 47.9 (NCH_2), 64.1 (CH_2), 103.0 (quat.), 110.1 (CH), 115.8 (CH), 121.6 (CH), 126.1 (quat.), 128.7 (2 × CH), 128.8 (2 × CH), 132.4 (quat.), 137.3 (quat.), 144.3 (CH), 147.5 (quat.), 148.8 (quat.), 149.1 (quat.), 150.7 (quat., C=O), 151.4 (quat.), 153.5 (quat., C=O); Anal. Calcd for $C_{23}H_{23}ClN_6O_4$: C, 57.2; H, 4.8; N, 17.4. Found: C, 57.2; H, 4.8; N, 17.3.

5.3.4.5. 8-{N′-[1-(3-Ethoxy-4-hydroxyphenyl)meth-(Z)-ylidene] hydrazino}-1,3-dimethyl-7-(2-nitrobenzyl)xanthine (2e).

Prepared from 3-ethoxy-4-hydroxybenzaldehyde **11b** (0.28 g, 1.67 mmol) and 8-hydrazino-1,3-dimethyl-7-(2-nitrobenzyl)-3,7-1*H*-dihydropurine-2,6-dione **10e** (0.52 g, 1.51 mmol), 8-{N′-[1-(3-ethoxy-4-hydroxyphenyl)meth-(*Z*)-ylidene]hydrazino}-1,3-dimethyl-7-(2-nitrobenzyl)-3,7-1*H*-dihydropurine-2,6-dione **2e** was obtained as dark orange crystals (0.29 g, 39%); R_f = 0.57 (ethyl acetate); mp 265–267 °C; ν_{max} (KBr)/cm^{-1} 3523 (NH), 3077 (OH), 1703 (C=O), 1627 (C=O), 1580 (Ar C=C), 1510 (NO_2), 1478 (Ar C=C), 1330 (NO_2), 1283 (C–O); ^{1}H NMR (300 MHz, DMSO): δ 1.27 (3H, t, J = 6.9 Hz, CH_3), 3.12 (3H, s, N^1-CH_3), 3.44 (3H, s, N^3-CH_3), 3.71 (2H, q, J = 6.9 Hz, CH_2), 6.06 (2H, s, CH_2), 6.70 (2H, s, H-5,6), 6.81 (1H, s, H-2), 7.00 (1H, dd, J = 8.4, 1.2 Hz, H-6), 7.55 (1H, m), 7.71 (1H, m), 7.85 (1H, s, CH), 8.20 (1H, dd, J = 8.1, 1.2 Hz, H-3), 9.80 (1H, bs, NH), 11.46 (1H, s, OH); ^{13}C NMR (75 MHz, DMSO): δ 14.5 (CH_3), 27.2 (CH_3), 29.4 (CH_3), 47.1 (NCH_2), 63.6 (CH_2), 102.5 (quat.), 106.7 (CH), 109.8 (CH), 115.4 (CH), 125.4 (CH), 124.9 (quat.), 128.4 (CH), 133.8 (quat.), 127.4 (CH), 127.6 (CH), 144.5 (CH), 146.6 (quat.), 147.0 (quat.), 148.7 (quat.), 149.4 (quat.), 151.6 (quat., C=O), 152.3 (quat.), 152.9 (quat., C=O); Anal. Calcd for $C_{23}H_{23}N_7O_6$: C, 56.0; H, 4.7; N, 19.9. Found: C, 55.7; H, 4.7; N, 19.8.

5.3.4.6. 7-(2-Ethoxycarbonylbenzyl)-8-{N′-[1-(3-ethoxy-4-hydroxyphenyl)meth-(*Z*)-ylidene]hydrazino}-1,3-dimethylxanthine (2f).

Prepared from 3-ethoxy-4-hydroxybenzaldehyde **11b** (0.25 g, 1.50 mmol) and 8-hydrazino-1,3-dimethyl-7-(1-ethoxycarbonyl benzyl)-3,7-1*H*-dihydropurine-2,6-dione **10g** (0.51 g, 1.37 mmol), 8-{N′-[1-(3-ethoxy-4-hydroxyphenyl)meth-(*Z*)-ylidene] hydrazino}-1,3-dimethyl-7-(1-ethoxycarbonylbenzyl)-3,7-1*H*-di hydropurine-2,6-dione **2f** was obtained as a fine white powder (0.55 g, 78%); mp 277–278 °C; ν_{max} (KBr)/cm^{-1} 3679 (NH). 3458 (OH), 1698 (C=O), 1654 (C=O), 1627 (C=O), 1580 (Ar C=C), 1478 (Ar C=C), 1261 (C–O); ^{1}H NMR (300 MHz, DMSO): δ 1.28 (3H, t, J = 6.9 Hz, CH_3), 1.34 (3H, t, J = 6.9 Hz, CH_3), 3.12 (3H, s, N^1-CH_3), 3.44 (3H, s, N^3-CH_3), 3.71 (2H, q, J = 6.9 Hz, CH_2), 4.34 (2H, q, J = 6.9 Hz, CH_2), 6.10 (2H, s, CH_2), 6.67–6.77 (4H, m), 7.40 (1H, m, H-4′), 7.53 (1H, m, H-5′), 7.83 (1H, s, CH), 8.01 (1H, dd, J = 7.8, 1.5 Hz, H-3′), 9.29 (1H, bs, NH), 11.50 (1H, s, OH); ^{13}C NMR (75 MHz, DMSO: δ 14.6 (CH_3), 15.0 (CH_3), 27.7 (CH_3), 29.9 (CH_3), 55.2 (NCH_2), 61.3 (CH_2), 64.2 (CH_2), 103.1 (quat.), 108.9 (CH), 115.9 (CH), 121.4 (CH), 126.0 (CH), 127.6 (CH), 128.7 (quat.), 131.0 (CH), 133.5 (CH), 139.5 (quat.), 144.2 (CH), 147.5 (quat.), 148.7 (quat.), 148.8 (quat.), 149.0 (quat.), 151.0 (quat., C=O), 151.5 (quat.), 152.5 (quat., C=O), 166.7 (quat., C=O); Anal. Calcd for $C_{26}H_{28}O_6N_6$: C, 60.0; H, 5.4; N, 16.1. Found: C, 60.0; H, 5.5; N, 16.3.

5.3.4.7. 7-Benzyl-8-{N′-[1-(3,4,5-triethoxyphenyl)meth-(*Z*)-ylidene]hydrazino}-1,3-dimethylxanthine (2h).

Prepared from 3,4,5-triethoxybenzaldehyde **11a** (0.71 g, 2.97 mmol) and 7-benzyl-8-hydrazino-1,3-dimethyl-3,7-1*H*-dihydro purine-2,6-dione **10a** (0.81 g, 2.69 mmol), 7-benzyl-1,3-dimethyl -8-{N‘-[1-(3,4,5-triethoxyphenyl)meth-(*Z*)-ylidene] hydrazino}-3, 7-1*H*-dihydropurine-2,6-dione **2h** was obtained as fine dark yellow crystals (0.63 g, 45%); R_f = 0.50 (ethyl acetate); mp 199–200 °C; ν_{max} (KBr)/cm^{-1} 3223 (NH), 1690 (C=O), 1639 (C=O), 1618 (Ar C=C), 1498 (Ar C=C), 1121 (C–O); ^{1}H NMR (300 MHz, DMSO): δ 1.21 (3H, t, J = 6.9 Hz, CH_3), 1.29 (6H, t, J = 6.9 Hz, 2 × CH_3), 3.16 (3H, s, N^1-CH_3), 3.40 (3H, s, N^3-CH_3), 3.81 (4H, q, J = 6.9 Hz, 2 × CH_2), 3.94 (2H, q, J = 6.9 Hz, CH_2), 5.81 (2H, s, CH_2), 6.70 (2H, s, H-2′,6′), 7.18–7.34 (5H, m), 7.90 (1H, s, CH), 11.72 (1H, bs, NH); ^{13}C NMR (75 MHz, DMSO): δ 15.1 (2 × CH_3), 15.9 (CH_3), 27.8 (CH_3), 29.8 (CH_3), 48.6 (NCH_2), 64.4 (2 × CH_2), 68.4 (CH_2), 103.1 (quat.), 105.1 (2 × CH), 126.8 (2 × CH), 127.6 (CH), 128.9 (2 × CH), 129.9 (quat.), 138.4 (quat.), 138.7 (quat.), 143.4 (CH), 148.7 (quat.), 150.3 (quat.), 151.4 (quat., C=O), 153.1 (2 × quat.), 153.5 (quat., C=O); Anal. Calcd for $C_{27}H_{32}N_6O_5$: C, 62.3; H, 6.2; N, 16.1. Found: C, 62.4; H, 6.2; N, 16.2.

5.3.4.8. 8-{N′-[1-(3,4,5-Triethoxyphenyl)meth-(Z)-ylidene] hydrazino}-1,3-dimethyl-7-(4-nitrobenzyl)xanthine (2i).

Prepared from 3,4,5-triethoxybenzaldehyde **11a** (0.78 g, 3.29 mmol) and 8-hydrazino-1,3-dimethyl-7-(4-nitrobenzyl)-3,7-1*H*-dihydropurine-2,6-dione **10b** (1.00 g, 2.90 mmol), 1,3-dimethyl-7-(4-nitrobenzyl)-8-{N′-[1-(3,4,5-triethoxyphenyl)meth-(*Z*)-ylidene]hydrazino}-3,7-1*H*-dihydropurine-2,6-dione **2i** was obtained as a pale yellow solid (0.12 g, 7%); R_f = 0.41 (ethyl acetate); mp 187–190 °C; ν_{max} (KBr)/cm^{-1} 3334 (NH), 1681 (C=O), 1619 (C=O), 1575 (Ar C=C), 1530 (NO_2), 1499 (Ar C=C), 1338 (NO_2), 1126 (C–O); ^{1}H NMR (300 MHz, DMSO): δ 1.13 (3H, t, J = 6.9 Hz, CH_3), 1.17 (6H, t, J = 6.9 Hz, 2 × CH_3), 3.05 (3H, s, N^1-CH_3), 3.32 (3H, s, N^3-CH_3), 3.71 (4H, q, J = 6.9 Hz, 2 × CH_2), 3.82 (2H, q, J = 6.9 Hz, 2 × CH_2), 5.81 (2H, s, CH_2), 6.54 (2H, s, H-2′,6′), 7.38 (2H, d, J = 8.7 Hz, H-2,6), 7.92 (1H, s, CH), 8.12 (2H, d, J = 8.7 Hz, H-3,5), 11.90 (1H, bs, NH); ^{13}C NMR (75 MHz, DMSO): δ 15.1 (2 × CH_3), 15.9 (CH_3), 27.7 (CH_3), 29.9 (CH_3), 48.6 (NCH_2), 64.2 (2 × CH_2), 68.5 (CH_2), 105.2 (CH), 107.1 (quat.), 124.1

(2 × CH), 127.9 (2 × CH), 129.8 (quat.), 139.4 (quat.), 144.0 (CH), 147.1 (quat.), 148.7 (quat.), 148.8 (quat.), 150.6 (quat.), 151.5 (quat., C=O), 153.1 (2 × quat.), 153.5 (quat., C=O); Anal. Calcd for $C_{27}H_{31}N_7O_7$: C, 57.3; H, 5.5; N, 17.3. Found: C, 57.0; H, 5.2; N, 17.0.

5.3.4.9. 8-{N′-[1-(3,4,5-Triethoxyphenyl)meth-(*Z*)-ylidene] hydrazino}-1,3-dimethyl-7-(4-methylbenzyl)xanthine (2j).

Prepared from 3,4,5-triethoxybenzaldehyde **11a** (0.84 g, 3.52 mmol) and 8-hydrazino-1,3-dimethyl-7-(4-methylbenzyl)-3,7-1*H*-dihydropurine-2,6-dione **10c** (0.99 g, 3.19 mmol), 1,3-dimethyl-7-(4-methylbenzyl)-8-{N'-[1-(3,4,5-triethoxyphenyl) meth-(*Z*)-ylidene]hydrazino}-3,7-1*H*-dihydropurine-2,6-dione **2j** was obtained as a cream solid (1.16 g, 68%); R_f = 0.52 (ethyl acetate); mp 216–219 °C; ν_{max} (KBr)/cm^{-1} 3244 (NH), 1692 (C=O), 1653 (C=O), 1622 (Ar C=C), 1501 (Ar C=C), 1126 (C–O); ^{1}H NMR (300 MHz, DMSO): δ 1.21 (3H, t, J = 6.9 Hz, CH_3), 1.29 (6H, t, J = 6.9 Hz, 2 × CH_3), 2.24 (3H, s, CH_3), 3.16 (3H, s, N^1-CH_3), 3.40 (3H, s, N^3-CH_3), 3.84 (4H, q, J = 6.9 Hz, 2 × CH_2), 3.94 (2H, q, J = 6.9 Hz, 2 × CH_2), 5.75 (2H, s, CH_2), 6.73 (2H, s, H-2′,6′), 7.06-7.13 (4H, m), 7.91 (1H, s, CH), 11.69 (1H, bs, NH); ^{13}C NMR (75 MHz, DMSO): δ 15.1 (2 × CH_3), 15.9 (CH_3), 21.1 (CH_3), 27.8 (CH_3), 29.8 (CH_3), 48.4 (NCH_2), 64.4 (2 × CH_2), 68.4 (CH_2), 103.1 (quat.), 105.1 (2 × CH), 126.9 (2 × CH), 129.5 (2 × CH), 129.9 (quat.), 135.3 (quat.), 136.7 (quat.), 138.7 (quat.), 143.4 (CH), 148.7 (quat.), 150.3 (quat.), 151.5 (quat., C=O), 153.1 (2 × quat.), 153.5 (quat., C=O); Anal. Calcd for $C_{28}H_{34}O_5N_6$: C, 62.9; H, 6.4; N, 15.7. Found: C, 63.2; H, 6.5; N, 15.6.

5.3.4.10. 8-{N′-[1-(3,4,5-Triethoxyphenyl)meth-(*Z*)-ylidene] hydrazino}-1,3-dimethyl-7-(2-methoxybenzyl)xanthine (2k).

Prepared from 3,4,5-triethoxybenzaldehyde **11a** (0.81 g, 3.40 mmol) and 8-hydrazino-1,3-dimethyl-7-(2-methoxybenzyl)-3,7-1*H*-dihydropurine-2,6-dione **10f** (1.06 g, 3.20 mmol), 1,3-dimethyl-7-(2-methoxybenzyl)-8-{N'-[1-(3,4,5-triethoxyphenyl)-meth(*Z*)-ylidene]hydrazino}-3,7-1*H*-dihydropurine-2,6-dione **2k** was obtained as fine yellow crystals (0.87 g, 83%); R_f = 0.50 (ethyl acetate); mp 224–228 °C; ν_{max} (KBr)/cm^{-1} 3221 (NH), 1694 (C=O), 1639 (C=O), 1622 (Ar C=C), 1496 (Ar C=C), 1120 (C–O); ^{1}H NMR (300 MHz, DMSO): δ 1.20 (3H, t, J = 6.9 Hz, CH_3), 1.30 (6H, t, J = 6.9 Hz, 2 × CH_3), 3.13 (3H, s, N^1-CH_3), 3.43 (3H, s, N^3-CH_3), 3.82 (3H, s, OCH_3), 3.84–4.10 (6H, m, 3 × CH_2), 5.71 (2H, s, CH_2), 6.57 (1H, d, J = 7.8 Hz, H-3), 6.64 (2H, s, H-2′,6′), 6.84 (1H, m, H-5), 7.02 (1H, d, J = 7.8 Hz, H-6), 7.22 (1H, m, H-4), 7.87 (1H, s, CH), 11.59 (1H, bs, NH); ^{13}C NMR (75 MHz, DMSO): δ 15.2 (2 × CH_3), 15.9 (CH_3), 27.7 (CH_3), 29.9 (CH_3), 44.8 (NCH_2), 55.9 (OCH_3), 64.5 (2 × CH_2), 68.5 (CH_2), 103.2 (quat.), 105.3 (2 × CH), 110.9 (CH), 120.9 (CH), 125.7 (CH), 126.3 (quat.), 128.4 (CH), 129.9 (quat.), 138.8 (quat.), 143.5 (CH), 148.7 (quat.), 150.9 (quat.), 151.5 (quat., C=O), 153.1 (2 × quat.), 153.4 (quat., C=O), 156.3 (quat.); Anal. Calcd for $C_{28}H_{34}O_6N_6$: C, 61.1; H, 6.2; N, 15.3. Found: C, 60.8; H, 6.2; N, 15.0.

5.3.4.11. 7-(2-Ethoxycarbonylbenzyl)-8-{N′-[1-(3,4,5-triethoxyphenyl)meth-(*Z*)-ylidene]hydrazino}-1,3-dimethylxanthine (2l).

Prepared from 3,4,5-triethoxybenzaldehyde **11a** (0.36 g, 1.49 mmol) and 8-hydrazino-1,3-dimethyl-7-(1-ethoxycarbonyl benzyl)-3,7-1*H*-dihydropurine-2,6-dione **10g** (0.50 g, 1.35 mmol), 1,3-dimethyl-7-(1-ethoxycarbonylbenzyl)-8-{*N*'-[1-(3,4,5-triethoxyphenyl)meth-(*Z*)-ylidene]hydrazino}-3,7-1*H*-dihydropurine-2, 6-dione **2l** was obtained as a white solid (0.56 g, 70%); mp 227–228 °C; ν_{max} (KBr)/cm^{-1} 3599 (NH), 1696 (C=O), 1648 (C=O), 1622 (C=O), 1577 (Ar C=C), 1467 (Ar C=C), 1122 (C–O); ^{1}H NMR (300 MHz, DMSO): δ 1.19 (3H, t, J = 6.9 Hz, CH_3), 1.28 (6H, t, J = 6.9 Hz, 2 × CH_3), 1.33 (2H, t, J = 6.9 Hz, CH_3), 3.11 (3H, s, N^1-CH_3), 3.44 (3H, s, N^3-CH_3), 3.77 (4H, q, J = 6.9 Hz, 2 × CH_2), 3.90 (2H, q, J = 6.9 Hz, CH_2), 4.33 (2H, q, J = 7.2 Hz, CH_2), 6.1 (2H, s, CH_2), 6.56 (2H, s, H-2′,6′), 6.79 (1H, d, J = 7.5 Hz, H-6), 7.39 (1H, m, H-4), 7.54 (1H, m, H-5), 7.88 (1H, s, CH), 8.00 (1H, dd, J = 7.5, 1.2 Hz, H-3), 11.74 (1H, bs, NH); ^{13}C NMR (75 MHz, DMSO): δ 14.6 (CH_3), 15.1 (2 × CH_3), 15.9 (CH_3), 27.7 (CH_3), 29.9 (CH_3), 48.4 (NCH_2), 61.3 (CH_2), 64.4 (2 × CH_2), 68.4 (CH_2), 103.2 (quat.), 105.1 (2 × CH), 126.1 (CH), 127.4 (CH), 127.7 (quat.), 129.8 (quat.), 130.9 (CH), 133.5 (CH), 138.7 (quat.), 140.4 (quat.), 143.7 (CH), 148.7 (quat.), 150.8 (quat.), 151.5 (quat., C=O), 153.1 (2 × quat.), 153.4 (quat., C=O), 166.7 (quat., C=O); Anal. Calcd for $C_{30}H_{36}O_7N_6$: C, 60.8; H, 6.1; N, 14.2. Found: C, 60.6; H, 6.0; N, 13.9.

5.3.5. General procedure for the synthesis of 7-(1-carboxybenzyl)-8-{*N*′-[1-(3-ethoxy-4-hydroxyphenyl)meth-(*Z*)-ylidene]hydrazino}-1,3-dimethylxanthine (2g) and 7-(1-carboxybenzyl)-8-{*N*′-[1-(3,4,5-triethoxyphenyl)meth-(*Z*)-ylidene]hydrazino}-1,3-dimethylxanthine (2m)

To a suspension of **2f** or **2l**, (0.64 mmol) in methanol (20 mL), a solution of lithium hydroxide (0.03 g, 1.34 mmol) in distilled water (10 mL) was added and the mixture refluxed for 3 h. The solvent was evaporated under reduced pressure. The resulting solid residue was dissolved in distilled water (20 mL), then acidified with 1% aq. HCl. The precipitated solid was filtered, dried in a vacuum oven, then recrystallized from methanol and acetonitrile to give **2g** or **2m**, respectively.

5.3.5.1. 7-(2-Carboxybenzyl)-8-{N′-[1-(3-ethoxy-4-hydroxyphenyl)meth-(Z)-ylidene]hydrazino}-1,3-dimethylxanthine (2g).

Prepared from 8-{*N*′-[1-(3-ethoxy-4-hydroxyphenyl)-meth-(*Z*)-ylidene]hydrazino}-1,3-dimethyl-7-(1-ethoxycarbonylbenzyl)-3,7-1*H*-dihydropurine-2,6-dione **2f** (0.33 g, 0.64 mmol), 8-{*N*′-[1-(3-ethoxy-4-hydroxyphenyl)meth-(*Z*)-ylidene]hydrazino}-1,3-dimethyl-7-(1-carboxybenzyl)-3,7-1*H*-dihydropurine-2,6-dione **2g** was obtained as a fine pink solid (0.03 g, 10%); mp 285–286 °C; ν_{max} (KBr)/cm^{-1} 3234 (NH), 3105 (OH), 17.17 (C=O), 1679 (C=O), 1619 (C=O), 1579 (Ar C=C), 1477 (Ar C=C), 1200 (C–O); ^{1}H NMR (300 MHz, DMSO): δ 1.20 (3H, t, J = 6.9 Hz, CH_3), 1.98 (1H, s, OH), 3.03 (3H, s, N^1-CH_3), 3.37 (3H, s, N^3-CH_3), 3.59 (2H, q, J = 6.9 Hz, CH_2), 6.02 (2H, s, CH_2), 6.58–6.66 (4H, m), 7.27 (1H, m, H-4′), 7.42 (1H, m, H-5′), 7.74 (1H, s, CH), 7.91 (1H, dd, J = 7.5, 1.5 Hz, H-3′), 9.18 (1H, bs, NH), 11.46 (1H, s, OH); ^{13}C NMR (75 MHz, DMSO): δ 15.0 (CH_3), 27.7 (CH_3), 29.9 (CH_3), 48.7 (NCH_2), 64.1 (CH_2), 103.1 (quat.), 110.2 (CH), 115.9 (CH), 121.5 (CH), 126.0 (CH), 127.2 (CH), 124.9 (quat.), 131.2 (CH), 133.1 (CH), 140.6 (quat.), 144.1 (CH), 147.4 (quat.), 147.5 (quat.), 148.8 (quat.), 149.0 (quat.), 151.0 (quat., C=O), 151.5 (quat.), 153.3 (quat., C=O,), 168.6 (quat., C=O); Anal. Calcd for $C_{24}H_{24}N_6O_6$: C, 58.5; H, 4.9; N, 17.1. Found: C, 58.4; H, 4.9; N, 16.9.

5.3.5.2. 7-(2-Carboxybenzyl)-8-{N′-[1-(3,4,5-triethoxyphenyl) meth-(Z)-ylidene]hydrazino}-1,3-dimethylxanthine (2m).

Prepared from 1,3-dimethyl-7-(1-ethoxycarbonylbenzyl)-8-{*N*'-[1-(3,4,5-triethoxy phenyl)meth-(*Z*)-ylidene]hydrazino}-3,7-1*H*-dihydropurine-2,6-dione **2l** (0.34 g, 0.57 mmol), 1,3-dimethyl-7-(1-carboxybenzyl)-8-{*N*'-[1-(3,4,5-triethoxyphenyl)meth-(*Z*)-ylidene]hydrazino}-3,7-1*H*-dihydropurine-2,6-dione **2m** was obtained as a yellow solid (0.12 g, 36%); mp 259–260 °C; ν_{max} (KBr)/cm^{-1} 3223 (NH), 3119 (OH), 1714 (C=O), 1679 (C=O), 1615 (C=O), 1574 (Ar C=C), 1472 (Ar C=C), 1121 (C–O); ^{1}H NMR (300 MHz, DMSO): δ 1.19 (3H, t, J = 6.9 Hz, CH_3), 1.28 (6H, t, J = 6.9 Hz, 2 × CH_3), 3.11 (3H, s, N^1-CH_3), 3.44 (3H, s, N^3-CH_3), 3.78 (4H, q, J = 6.9 Hz, 2 × CH_2), 3.90 (2H, q, J = 6.9 Hz, CH_2), 6.11 (2H, s, CH_2), 6.55 (2H, s, H-2′,6′), 6.77 (1H, d, J = 7.8 Hz, H-6), 7.37 (1H, m, H-4), 7.50 (1H, m, H-5), 7.88 (1H, s, CH), 8.00 (1H, dd, J = 7.8, 1.5 Hz, H-3), 11.81 (1H, bs, NH); ^{13}C NMR (75 MHz, DMSO): δ 15.1 (2 × CH_3), 15.9 (CH_3), 27.7 (CH_3), 29.9 (CH_3), 48.6 (NCH_2),

64.4 (2 × CH_2), 68.4 (CH_2), 103.1 (quat.), 105.0 (2 × CH), 125.9 (CH), 127.2 (CH), 129.8 (quat.), 131.2 (CH), 131.6 (quat.), 133.1 (CH), 138.7 (quat.), 140.4 (quat.), 143.7 (CH), 148.7 (quat.), 150.8 (quat.), 151.5 (quat., C=O), 153.1 (2 × quat.), 153.3 (quat., C=O), 168.6 (quat., C=O); Anal. Calcd for $C_{28}H_{32}O_7N_6$: C, 59.6; H, 5.7; N, 14.9. Found: C, 59.5; H, 5.7; N, 14.8.

5.4. Biological testing

5.4.1. Cell culture

Cells were seeded in 96 well microtiter plates at an optimal density so that the untreated cells were in the exponential growth phase at the time of harvest (10,000 cells/well which was the optimal cell density from preliminary studies). All the plates were incubated overnight to allow cell attachment. The 96 well plates were set up with six in-plate replicates of eight concentrations of the drug. Control wells were treated with fresh media containing no drug. The same solvent (DMSO) used to dissolve the test compound was added to the control wells so that the concentration of the solvent present in all the wells was <1%. Wells were also set up with just the medium to serve as the negative control for the determination of any background absorbance that may be present. The absorbance (or fluorescence) levels from drug treated cells were corrected against untreated control absorbance (or fluorescence) values. All of the compounds tested were soluble at all concentrations and did not interfere with the colorimetric assay chemistry. Assays were based on comparative growth with the control, set as 100% growth. The IC_{50} was defined as 50% reduction of absorbance.

Normal human epidermal keratinocytes (Promocell; NHEK pooled adult) were grown in keratinocyte growth medium (Promocell), with the growth supplement (supplied with the medium) consisting of insulin, hydrocortisone, transferrin, epinephrine, bovine pituitary extract, and epidermal growth factor. Trypsinization was performed using the detach kit C-14200, Promocell) recommended by the supplier. The HPV-16 transformed human keratinocyte cell line, CCD-1106, was cultured in serum free medium (GIBCO) with the growth supplement (supplied with the medium) consisting of L-glutamine, bovine pituitary extract, and epidermal growth factor. HaCaT cells were grown in Dulbecco's modified Eagle's medium (GIBCO) supplemented with 10% fetal bovine serum and 2 mM L-glutamine.

The human monocytic cell lines, THP-1 and U937, were grown in RPMI medium (GIBCO) supplemented with 10% fetal bovine serum and 2 mM L-glutamine.

Streptomycin (100 μg/mL) and penicillin (100 U/mL) were also added to the media.

5.4.1.1. MTT assay. The MTT assay was performed according to the method developed by Mosmann.[54] After the 72 h incubation period, cells in 96 well plates were exposed to 200 μl of MTT (0.5 mg/ml in PBS) and incubated for 2 h at 37 °C/5% CO_2. The cells were washed with PBS after the removal of the dye and 200 μl of 90% isopropanol/10% DMSO was added to the plates. The plates were incubated in the dark for 10 min and the absorbance at 590 nm was recorded immediately using a microplate reader (Tecan, Reading, UK).

5.4.1.2. Cell Titer 96 Aqueous One solution assay. Cells were seeded in round bottomed 96 well microtiter plates at 10,000 cells/well and exposed to the test compounds for 72 h. At the end of the incubation period, the Cell titer 96 Aqueous One solution cell proliferation assay was used to determine the growth inhibitory effects of the compounds, with the assay performed according to the manufacturer's instructions. After the addition of the reagent, the plates were incubated for 3 h at 37 °C. Formazan formation was determined using a microplate reader at 492 nm.

5.4.1.3. Cyto Tox 96 cytotoxicity assays. The Cyto Tox 96 assay was performed following the manufacturer's (Promega) protocol.

5.4.2. Effect of inhibitors on protein levels in CCD-110 cells

Cells were grown on 6-well plates and were exposed to vehicle, EGF or novel compounds (added from stock solutions dissolved in medium/DMSO 1:1 or DMSO, for 30 min) for the required period of time, at 37 °C,and then placed on ice to stop the reaction. Cells were then washed with PBS (2 × 1 mL). For cross-linking assays, BS^3 (500 μl) was then added for 30 min at room temperature, the reaction was quenched with 10 μL 1 M Tris 20 mM (pH 7.5) for 15 min at room temperature, then washed with PBS (2 × 1 mL) before 250 μl of 4 × sample buffer [63 mM Tris–HCl, pH 6.8, 2 mM $Na_4P_2O_7$, 5 mM EDTA, 10% (v/v) glycerol, 2% (w/v) SDS, 50 mM DTT, 0.007% (w/v) bromophenol blue] was added. The cells were then scraped and dispensed into Eppendorf tubes using a gauge needle, a hole was impregnated in each of the sample lids and the tubes were boiled for 5 min to denature the protein. The samples were then frozen and stored at −20 °C.

Resolving gels were prepared containing an appropriate amount [5% (w/v), 7.5% (w/v) or 10% (w/v)] acrylamide: N′-methylenebisacrylamide (30:0.8), 0.375 M tris pH 8.8, 0.1% (w/v) SDS and 0.05% (w/v) ammonium persulfate (APS). Polymerization was initiated by the addition of 0.05% (v/v) *N*,*N*,*N*′,*N*′-tetramethylethylenediamine (TEMED). The solution was poured between two glass plates, and overlayed with 200 μL 0.1% (w/v) SDS. After polymerization, a stacking gel containing 10% (v/v) acrylamide: N′-methylenebisacrylamide (30:0.8) in 125 mM tris, pH 6.8, 0.1% (w/v) SDS, 0.05% (w/v) ammonium persulfate and 0.05% (v/v) TEMED was poured directly on top of the resolving gel, and a comb inserted. After polymerization was complete the comb was removed and the polyacrylamide gels were assembled in a Bio-Rad Mini-PROTEAN II™ electrophoresis tank, with both reservoirs filled with electrophoresis buffer (25 mM tris, 192 mM glycine, 0.1% (w/v) SDS). Aliquots of samples (10–30 μL) from the cell lysates were loaded into the wells using a microsyringe. A prestained SDS–PAGE molecular weight marker of known molecular weights was run to identify the polypeptide of interest. Samples were electrophoresed at a constant voltage (90–150 V), for 90 min or until the bromophenol blue dye reached the bottom of the gel.

The proteins separated by SDS–PAGE were transferred to nitrocellulose membranes by electrophoretic blotting. The gel was pressed firmly against a nitrocellulose sheet and assembled in a transfer cassette sandwiched between Whatmann 3MM paper and two sponge pads. The cassette was immersed in blotting buffer (25 mM Tris, 195 mM glycine, 20% (v/v) methanol) in a Bio-Rad Mini Trans-Blot™ tank and a constant current of 0.3–0.4 Å was applied for 2–5 h whilst the tank was cooled by inclusion in an ice reservoir.

Following transfer of the proteins to the nitrocellulose membrane, the membrane was removed and any remaining protein blocked by incubation in a solution of 3% (w/v) BSA in NaTT (150 mM NaCl, 20 mM Tris, pH 7.4, 0.2% (v/v) Tween-20) for 2 h. Blocking buffer was then replaced with a solution of 0.2% (w/v) BSA in NaTT and an appropriate volume (1–5 μL) of the antibody specific for the protein of interest was added. This mixture was agitated overnight and then washed every 15 min for 1.5–2 h in NaTT. A secondary antibody (1–2 μL) directed against the primary antibody, was then added in 0.2% (w/v) BSA solution and incubated for a further 2 h prior to further washing every 15 min over a 1.5 h period. The membranes were then exposed to an enhanced chemiluminescence (ECL) reagent for 1.5 min with agitation before

being placed in an exposure cassette and covered with Saran-wrap™. Blots were then exposed to Kodak X-OMAT LS film for 2–5 min under darkroom conditions and were then developed using a Kodak M35-M X-OMAT processor.

Densitometry measurements were recorded using *Scion image* for Windows, 2000–2001, Scion corporation, Alpha 4.0.3.2.

5.4.2.1. Effect of inhibitors on EGFR dimerization. Cells were exposed to varying concentrations of the test compounds for 30 min, then stimulated with EGF at 50 ng/mL for 10 min at 37 °C, and cross-linked with BS^3 at 2 mM for 30 min at room temperature. After solubilization and SDS–page gel electrophoresis, the samples were transferred onto nitrocellulose paper and then immunoblotted with anti-EGFR antibodies. In the absence of cross-linker, the dimers separate into monomers upon SDS–page gel electrophoresis.[55] The protein species at 170 kDa is proposed to be the EGFR monomer and at the 340 kDa, the covalently linked dimer. It is assumed during the procedure that both the monomer and dimer are equally transferred onto the nitrocellulose paper and that the both species exhibit equal recognition by the anti-EGFR antibodies. Immunoblots were quantified by densitometry as optical density (% control).

5.4.2.2. Effect of inhibitors on levels of phosphorylated downstream proteins. Cells were exposed to compounds for 30 min, then EGF (100 ng/mL) for 10 min. The immunoblots p-ERK 1 (44 kDa), p-ERK 2 (42 kDa) and p-p38 were representative of one experiment and were quantified by densitometry as optical density (% control).

5.4.3. Assay of caspase-3/7 activity

Cells were plated in 96 well plates at 10^4 cells/well and exposed to different concentrations of the drug as described earlier. Control wells were treated with fresh media containing no drug. Wells were also set up with the medium alone to serve as the negative control for the determination of any background fluorescence that may be present. Each sample was analysed in triplicate. After the desired incubation period, the caspase-3/7 activity was measured using the Apo-ONE homogeneous caspase-3/7 assay kit (Promega) according to the manufacturer's instructions. Fluorescence was measured at 499/521 nm using a Flex station (Invitrogen, Paisley, UK).

5.4.4. Annexin V-FITC/propidium iodide (PI) FACS apoptosis assay

Flow cytometric determination of apoptosis was carried out as previously described.[56] Following treatment of 10^6 cells with different concentrations of the test compound for the desired incubation period, the cells were harvested, washed once in ice-cold PBS and incubated with Annexin V-FITC and PI as recommended by the manufacturer. Cells incubated with the medium alone were used as a negative control. Samples were analysed immediately on a FACS SCAN flow cytometer (Becton Dickinson) using the standard optics for detecting FL1 (FITC) and FL2 (PI). All samples were run in triplicate. Ten thousand events were collected per sample using flow cytometry and debris was excluded by scatter gating. Single Annexin V-FITC and PI stained samples as well as no-dye-negative control samples determined quadrants for data analysis. The data was analyzed by WINMDI software (Becton Dickinson, Canada) and the percentage of cells in viable, early apoptotic and late apoptotic quadrants were calculated. Three keratinocyte sub-populations could be discriminated; (a) annexin-V-negative/PI negative, i.e. viable cells, (b) annexin-V-positive/PI negative, i.e. early-phase apoptotic cells, and (c) annexin-V-positive/PI positive, i.e. late-phase apoptotic cells.

5.4.5. Anti-oxidant assay

Exact details of the anti-oxidant assay can be found in a separate study.[22]

Acknowledgements

We thank Stiefel International R&D (now Stiefel, a GSK company) for sponsoring this research.

Supplementary data

Supplementary data associated with this article can be found, in the online version, at http://dx.doi.org/10.1016/j.bmc.2012.07.048.

References and notes

1. McKay, I. A.; Leigh, I. M. *Clin. Dermatol.* **1995**, *13*, 105.
2. Sharma, V.; Orchard, D. *Paediatr Child Health* **2011**, *21*, 126.
3. Clark, C. M.; Chalmers, R. J. G.; Rowe, P. H.; Li, W. P. A.; Williams, H. C.; Griffiths, C. E. M. A. *Brit. J. Dermatol.* **2001**, *145*, 40.
4. Mendonca, C. O.; Burden, A. D. *Pharmacol. Ther.* **2003**, *99*, 133.
5. Feldman, S. R.; Evans, C.; Russell, M. W. *J. Dermatol. Treat.* **2005**, *16*, 37.
6. Chaplin, S.; Downs, T. *Prescriber* **2009**, *20*, 29.
7. Talamonti, M.; Spallone, G.; Di Stefani, A.; Costanzo, A.; Chimenti, S. *Expert Opin. Drug Safety* **2011**, *10*, 239.
8. Nanney, L. B.; Stoscheck, C. M.; Maagid, M.; King, L. E. *J. Invest. Dermatol.* **1986**, *86*, 260.
9. Varani, J.; Kang, S.; Stoll, S.; Elder, J. T. *Pathobiology* **1998**, *66*, 253.
10. Varani, J.; Lateef, H.; Fay, K.; Elder, J. T. *Skin Pharmacol. Physiol.* **2005**, *18*, 123.
11. Mascia, F.; Cataisson, C.; Lee, T. C.; Threadgill, D.; Mariani, V.; Amerio, P.; Chandrasekhara, C.; Adeva, G. S.; Girolomoni, G.; Yuspa, S. H.; Pastore, S. *J. Invest. Dermatol.* **2010**, *130*, 682.
12. Abd El-Rehim, D. M.; Pinder, S. E.; Paish, C. E.; Bell, J. A.; Rampaul, R. S.; Blamey, R. W.; Robertson, J. F. R.; Nicholson, R. I.; Ellis, I. O. *Br. J. Cancer* **2004**, *91*, 1532.
13. Shama, S. V.; Bell, D. W.; Settelman, J.; Haber, D. A. *Nat. Rev. Cancer* **2007**, *7*, 169.
14. Peus, D.; Hamacher, L.; Pittelkow, M. R. *J. Invest. Dermatol.* **1997**, *109*, 751.
15. (a) Powell, T. J.; Ben-Bassat, H.; Klein, B. Y.; Chen, H.; Shenoy, N.; McCollough, J.; Narog, B.; Gazit, A.; Harzstark, Z.; Chaouat, M.; Levtizki, R.; Tang, C.; McMahon, J.; Shawver, L.; Levitzki, A. *Br. J. Dermatol.* **1999**, *141*, 802; (b) Ben-Bassat, H.; Klein, B. Y. *Curr. Pharm. Des.* **2000**, *6*, 933; (c) Ben-Bassat, H.; Vardi, D. V.; Gazit, A.; Klaus, S. N.; Chaouat, M.; Hartzstark, Z.; Levtizki, A. *Exp. Dermatol.* **1995**, *4*, 82.
16. Giroux-Leprieur, E.; Friard, S.; Couderc, L.-J. *Eur. J. Dermat.* **2010**, *20*, 243.
17. Wierzbicka, E.; Tourani, J. M.; Guillet, G. *Br. J. Dermatol.* **2006**, *155*, 207.
18. Trivin, F.; Boucher, E.; Raoul, J.-L. *Acta Oncol.* **2004**, *43*, 592.
19. Choong, N. W.; Cohen, E. E. W. *Crit. Rev. Oncology/Hematology* **2006**, *57*, 25.
20. Ogiso, H.; Ishitani, R.; Nureki, O.; Fukai, S.; Yamanaka, M.; Kim, J. H.; Saito, K.; Inoue, M.; Shirouzu, M.; Yokoyama, S. *Cell* **2002**, *110*, 775.
21. Yang, R. Y. C.; Yang, K. S.; Pike, L. J.; Marshall, G. R. *Chem. Biol. Drug Des.* **2010**, *76*, 1.
22. Dodou, K.; Anderson, R. J.; Lough, W. J.; Small, D. A. P.; Shelley, M. D.; Groundwater, P. W. *Bioorg. Med. Chem.* **2005**, *13*, 4228.
23. Vollmann, K.; Müller, C. E. *Heterocycles* **2002**, *57*, 871.
24. George, S. E.; Anderson, R. J.; Cunningham, A.; Donaldson, M.; Groundwater, P. W. *ASSAY and Drug Develop Technol.* **2010**, *8*, 389.
25. Gottlieb, A. B.; Khandke, L.; Krane, F.; Staiano-Coico, L.; Ashinoff, R.; Krueger, J. G. *J. Invest Dermatol.* **1992**, *98*, 680.
26. Borenfreund, E.; Babich, H.; Martin-Alguacil, N. *Toxic. In vitro* **1988**, *2*, 1.
27. Hussain, R. F.; Nouri, A. M.; Oliver, R. T. *J. Immunol. Methods* **1993**, *160*, 89.
28. Garrett, T. P. J.; McKern, N. M.; Lou, M.; Elleman, T. C.; Adams, T. E.; Lovrecz, G. O.; Zhu, H.-J.; Walker, F.; Frenkel, M. J.; Hoyne, P. A.; Jorissen, R. N.; Nice, E. C.; Burgess, A. W.; Ward, C. W. *Cell* **2002**, *110*, 763.
29. Geronikaki, A. A.; Gavalas, A. M. *Comb. Chem. High Throughput Screen.* **2006**, *9*, 425.
30. Portugal, M.; Barak, V.; Ginsburg, I.; Kohen, R. *Biomed. Pharmacother.* **2007**, *61*, 412.
31. Wozniak, A.; Drewa, G.; Krzyzyńska-Malinowska, E.; Czajkowski, R.; Protas-Drozd, F.; MilaKierzen-kowska, C.; Rozwodowska, M.; Soponska, M.; Czarnecka-Zaba, E. *Med. Sci. Monit.* **2007**, *13*, CR30.
32. Heil, T. L.; Volkmamm, K. R.; Wataha, J. C.; Lockwood, P. E. *J. Oral Rehabil.* **2002**, *29*, 401.
33. Snyder, R. A.; Kaempfer, C. E.; Wintroub, B. U. *Blood* **1985**, *65*, 176.
34. Messmer, K.; Reynolds, G. P. *Neurosci. Lett.* **2005**, *388*, 93.
35. Mrowietz, U.; Jessat, H.; Schwarz, A.; Schwarz, T. *Br. J. Dermatol.* **1997**, *136*, 542.
36. Peus, D.; Beyerle, A.; Rittner, H. L.; Pott, M.; Meves, A.; Weyand, C.; Pittelkow, M. R. *J. Invest. Dermatol.* **2000**, *114*, 688.
37. Jeffes, E. W. B.; McCullough, J. L.; Pittelkow, M. R.; McCormick, A.; Almanzor, J.; Liu, G.; Dang, M.; Voss, K.; Voss, J.; Schlotzhauer, A.; Weinstein, G. D. *J. Invest. Dermatol.* **1995**, *104*, 183.
38. Cutolo, M.; Bisso, A.; Sulli, A.; Felli, L.; Briata, M.; Pizzomi, C.; Villaggio, B. *J. Rheumatol.* **2000**, *27*, 2551.

39. Holschermann, H.; Durfield, F.; Maus, U.; Bierhaus, A.; Heidinger, K.; Lohmeyer, J.; Nawroth, P. P.; Tillmans, H.; Haberbosch, W. *Blood* **1996**, *88*, 3837.
40. de Jong, E. C.; Vieira, P. L.; Kalinski, P.; Kapsenberg, M. L. *J. Leukocyte Biol.* **1999**, *66*, 201.
41. (a) Korting, H. C.; Schindler, S.; Hartinger, A.; Kerscher, M.; Angerpointner, T.; Maibach, H. I. *Life Sci.* **1994**, *55*, 533; (b) Seitz, M.; Zwicker, M.; Loetscher, P. *Arthritis Rheum.* **1998**, *41*, 2032.
42. Roche Applied Science. Apoptosis, Cell Death, and Cell Proliferation, 3rd Edn., (http://www.roche-applied-science.com/sis/apoptosis/docs/manual_apoptosis.pdf, last accessed 10th April 2012).
43. Bonnekoh, B.; Farkas, B.; Geisel, J.; Mahrle, G. *Arch. Dermatol. Res.* **1990**, *282*, 325.
44. Wrone-Smith, T.; Mitra, R. S.; Thompson, C. B.; Jasty, R.; Castle, V. P.; Nickoloff, B. J. *Amer. J. Pathology* **1997**, *151*, 1321.
45. Chen, S. H.; Arany, I.; Apisarnthanarax, N.; Rajaraman, S.; Tyring, S. K.; Horikoshi, T.; Brysk, H.; Brysk, M. M. *FASEB J.* **2000**, *14*, 565.
46. Bianchi, L.; Farrace, M. G.; Nini, G.; Piacentini, M. *J. Invest. Dermatol.* **1994**, *103*, 829.
47. Laporte, M.; Galand, P.; Fokan, D.; de Graef, C.; Heenen, M. *Dermatology* **2000**, *200*, 314.
48. Ruckert, R.; Asadullah, K.; Seifert, M.; Budagian, V. M.; Arnold, R.; Trombotto, C.; Paus, R.; Bulfone-Paus, S. *J. Immunol.* **2000**, *165*, 2240.
49. Itoh, K.; Kawasaki, S.; Kawamoto, S.; Seishima, M.; Chiba, H.; Michibata, H.; Wakimoto, K.; Imai, Y.; Minesaki, Y.; Otsuji, M.; Okubo, K. *Experim. Dermatol.* **2005**, *14*, 667.
50. Pirisi, L.; Creek, K. E.; Doniger, J.; DiPaolo, J. *Carcinogenesis* **1988**, *9*, 1573.
51. Pirisi, L.; Yasumoto, S.; Feller, M.; Doniger, J.; DiPaolo, J. A. *J. Virol.* **1987**, *61*, 1061.
52. Slotta, K. H.; Szyszka, G. *J. für Praktische Chemie* **1933**, *137*, 339.
53. Dolman, H.; van der Goot, J.; Moed, H. D. *Rec. Trav. Chim. Pays-Bas* **1965**, *84*, 193.
54. Mosmann, T. *J. Immunol. Methods* **1983**, *65*, 55.
55. Xiaochun, Y.; Sharma, K. D.; Takahashi, T.; Iwamoto, R.; Mekada, E. *Mol. Biol. Cell* **2002**, *13*, 2547.
56. Vermes, I.; Haanen, C.; Steffens-Nakken, H.; Reutelingsperger, C. *J. Immunol. Methods* **1995**, *184*, 39.